Resource

Cell Reports

Single-Cell RNA-Seq Reveals Hypothalamic Cell Diversity

Graphical Abstract

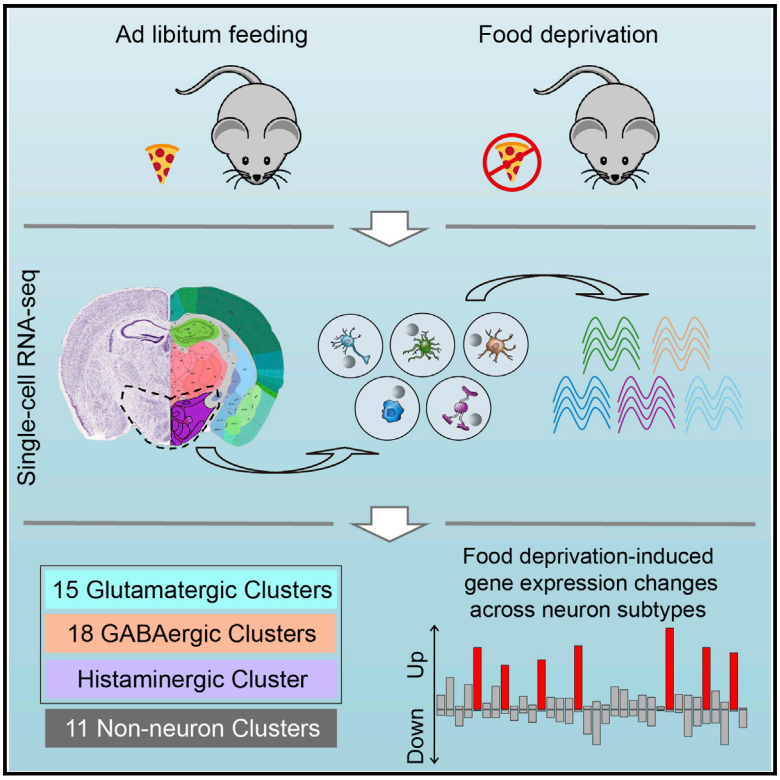

Authors

Renchao Chen, Xiaoji Wu, Lan Jiang, Yi Zhang

Correspondence

yzhang@genetics.med.harvard.edu

In Brief

Chen et al. perform single-cell RNA sequencing analysis of the adult mouse hypothalamus to probe the rich cell diversity of this complex brain region. They also identify neuronal subtype-specific transcriptional responses to food deprivation.

Highlights

- Transcriptome-based cell-type classification in mouse adult hypothalamus
- Transcriptional features of oligodendrocyte differentiation and tanycyte subtypes
- Neuropeptide and receptor expression patterns of hypothalamic neuronal subtypes
- Cell-type-specific transcriptional responses to food deprivation

Accession Numbers

GSE87544

Chen et al., 2017, Cell Reports *18*, 3227–3241
March 28, 2017
http://dx.doi.org/10.1016/j.celrep.2017.03.004

CellPress

Cell Reports
Resource

Single-Cell RNA-Seq Reveals Hypothalamic Cell Diversity

Renchao Chen,[1,2,3,6] Xiaoji Wu,[1,2,3,6] Lan Jiang,[1,2,3,6] and Yi Zhang[1,2,3,4,5,7,*]
[1]Howard Hughes Medical Institute, Boston Children's Hospital, Boston, MA 02115, USA
[2]Program in Cellular and Molecular Medicine, Boston Children's Hospital, Boston, MA 02115, USA
[3]Division of Hematology/Oncology, Department of Pediatrics, Boston Children's Hospital, Boston, MA 02115, USA
[4]Department of Genetics, Harvard Medical School, Boston, MA 02115, USA
[5]Harvard Stem Cell Institute, WAB-149G, 200 Longwood Avenue, Boston, MA 02115, USA
[6]Co-first author
[7]Lead Contact
*Correspondence: yzhang@genetics.med.harvard.edu
http://dx.doi.org/10.1016/j.celrep.2017.03.004

SUMMARY

The hypothalamus is one of the most complex brain structures involved in homeostatic regulation. Defining cell composition and identifying cell-type-specific transcriptional features of the hypothalamus is essential for understanding its functions and related disorders. Here, we report single-cell RNA sequencing results of adult mouse hypothalamus, which defines 11 non-neuronal and 34 neuronal cell clusters with distinct transcriptional signatures. Analyses of cell-type-specific transcriptomes reveal gene expression dynamics underlying oligodendrocyte differentiation and tanycyte subtypes. Additionally, data analysis provides a comprehensive view of neuropeptide expression across hypothalamic neuronal subtypes and uncover *Crabp1*$^{+}$ and *Pax6*$^{+}$ neuronal populations in specific hypothalamic subregions. Furthermore, we found food deprivation exhibited differential transcriptional effects among the different neuronal subtypes, suggesting functional specification of various neuronal subtypes. Thus, the work provides a comprehensive transcriptional perspective of adult hypothalamus, which serves as a valuable resource for dissecting cell-type-specific functions of this complex brain region.

INTRODUCTION

The hypothalamus is one of the most complex brain regions, essential for regulating physiological and behavioral homeostasis. Numerous studies have revealed its role in orchestrating a wide range of animal behaviors (Denton et al., 1996; Elmquist et al., 1999; Navarro and Tena-Sempere, 2011). Commensurate with its functional diversity, is its highly complex anatomical and cellular composition (Puelles and Rubenstein, 2015; Shimogori et al., 2010). Works in the last few decades have identified various cell types in hypothalamus based on different properties (Brown et al., 2013; Lee et al., 2015; Mathew, 2008; Wu et al., 2014). However, a comprehensive cell-type classification of hypothalamus has not been achieved.

Although different methodologies have been used for classifying cell types in the nervous system (Greig et al., 2013; Jiang et al., 2015), the most direct and unambiguous method to define a cell type is its transcriptional feature, as it underlies other cell features such as morphology, connectivity, and function (Greig et al., 2013; Toledo-Rodriguez et al., 2004). In addition, gene expression-based cell classification can be reliably and conveniently adapted by the entire research community (Gong et al., 2003), making data comparison among different groups possible. Indeed, a systematic in situ hybridization (ISH) database has revealed extensive cell-type heterogeneity in brain (Lein et al., 2007). However, the limitation of ISH on assessing co-expression of multiple genes prevents a definitive cell-type classification.

Recent advances in single-cell RNA sequencing (scRNA-seq) have facilitated the transcriptional cataloguing of cell types in many tissues, including those in the nervous system (Gokce et al., 2016; Macosko et al., 2015; Tasic et al., 2016; Zeisel et al., 2015). While cell diversity in the cerebral cortex (Lake et al., 2016; Tasic et al., 2016; Zeisel et al., 2015), hippocampus (Zeisel et al., 2015), and striatum (Gokce et al., 2016) has been cataloged to an unprecedented level, the cost and effort of profiling large numbers of single cells by conventional scRNA-seq methods prevent its broader application to highly complex brain regions, such as the hypothalamus. To overcome this challenge, cost-efficient scRNA-seq methods have been developed to achieve high-throughput parallel analysis (Klein et al., 2015; Macosko et al., 2015), making scRNA-seq analysis of complex brain regions possible.

Here, we applied high-throughput Drop-seq method (Macosko et al., 2015) to profile single cells dissociated from the adult mouse hypothalamus. Through clustering analysis, we identified 11 non-neuronal and 34 neuronal cell types. Data analysis revealed the transcriptional dynamics underlying the oligodendrocyte differentiation, as well as the transcriptional heterogeneity of tanycytes, a hypothalamus-specific non-neuronal cell type whose function remains poorly characterized. Additionally,

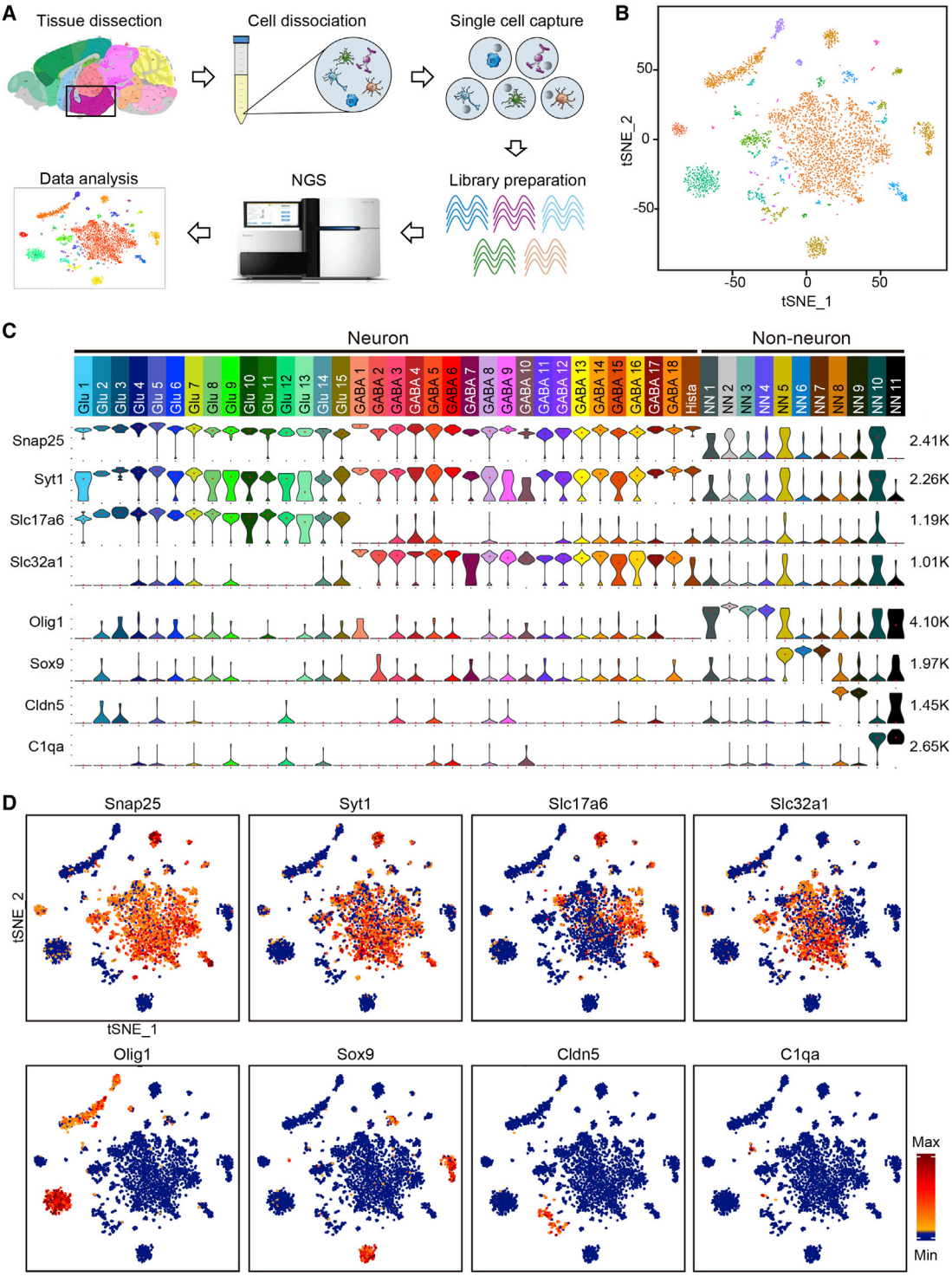

Figure 1. Identification of 45 Cell Types in Adult Mouse Hypothalamus by scRNA-Seq

(A) Workflow of single-cell RNA-seq of mouse hypothalamus. Hypothalamic tissues were dissected from adult mouse brain and dissociated into single-cell suspension. Single cells and barcoded beads were captured into droplets followed by cDNA synthesis, amplification, and library preparation. After next generation sequencing, cells were classified based on their transcriptomes.

(B) tSNE plot showing the overall gene expression relationship among the 3,319 single cells with more than 2,000 genes detected in each cell. Different cell clusters are color-coded.

(legend continued on next page)

single-cell transcriptome analysis revealed not only highly divergent expression patterns of neuropeptides and receptors across neuron subtypes, but also *Crabp1*$^+$ and *Pax6*$^+$ neuronal populations at specific hypothalamic regions. Furthermore, cell-type-specific transcription responses to food deprivation among various cell types were also revealed. Thus, our study provides a comprehensive gene expression map across divergent cell types in the hypothalamus, which will facilitate broader functional understanding of this complex brain region.

RESULTS

Overview of the Cell Types in Hypothalamus Identified by Single-Cell RNA-Seq

To characterize cellular heterogeneity in the hypothalamus, we performed scRNA-seq using cells dissociated from adult mouse hypothalamus (Figures 1A and S1A). In five independent experiments, we sequenced more than 14,000 single cells derived from dissociated hypothalamus tissues of seven mice. To assess the cell-type-specific transcriptional response to food-deprivation, four normal fed mice and three food-deprived (24 hr) mice were used. To increase cell number, and considering that 24 hr food-deprivation is a relatively mild treatment that unlikely to cause changes in cell identify, we combined the cells from both control and food-deprived mice for clustering analysis. From the 14,000 cells analyzed, 3,319 cells have more than 2,000 genes detectable in a single cell (Figure S1B). Semi-supervised clustering analysis (unsupervised clustering analysis [Macosko et al., 2015] followed by manually filtering [see the Experimental Procedures]) of the 3,319 cells (Figures S1C and S1D) identified 45 cell clusters with distinct gene expression signatures (Figures 1B and 1C). We applied the SC3 method to re-classify the same 3,319 cells (Kiselev et al., 2016) and found that the results were largely consistent (Figure S1E), demonstrating the reliability of our clustering results.

Based on the expression of the pan neuronal makers *Snap25* and *Syt1*, the 45 cell clusters were divided into 34 neuronal (*Snap25*/*Syt1*-high) and 11 non-neuronal clusters (*Snap25*/*Syt1*-negative or low) (Figures 1C and 1D). The 34 neuronal clusters could be further divided into 15 glutamatergic (Glu1–Glu15) and 18 GABAergic (GABA1–GABA18) subtypes based on their differential expression of *Slc17a6* and *Slc32a1* (Figures 1C and 1D). However, the ''Hista'' cluster did not belong to either of the two categories as neither *Slc17a6* nor *Slc32a1* was expressed in this cluster (Figure 1C). Among the non-neuronal clusters (NN1–NN11), *Olig01*, *Sox9*, *Cldn5*, and *C1qa* were highly expressed in NN1–NN4, NN5–NN7, NN8–NN9, and NN10–NN11, respectively (Figures 1C and 1D).

Based on the above clustering results, we re-assigned each of the 14,437 single cells ($\geq$800 transcripts detected) to the 45 cell clusters. We found that the cell number increased for each cluster (Table S1). Notably, more cells were categorized into non-neuronal clusters than neuronal clusters (Table S1), consistent with the fact that neurons express more genes than non-neuronal cells (Zeisel et al., 2015). Importantly, most of the 3,319 informative cells ($\geq$2,000 genes detected) were correctly assigned to the original clusters, and the pooled transcriptome of each cluster before and after adding the cells with <2,000 genes detected had a high Pearson's correlation coefficiency (Table S1), indicating that our clustering results based on the 3,319 cells could be reliably extended to the ~14,000 cells sequenced. Although some animals did not contribute to all of the 45 clusters, this is likely due to variations in tissue dissection, because each cluster includes cells from multiple animals and different treatments (Figure S1F), indicating that neither food deprivation nor different animals affects cell clustering.

Classification of Non-neuronal Cell Types in Hypothalamus

We generated gene expression heatmaps and identified marker genes for each of the non-neuronal clusters (Figures 2A and S2). The four *Oligo1*$^+$ oligodendrocyte clusters could be further distinguished from each other by the expression of *Top2a* (proliferating oligodendrocyte precursor cell [POPC]), *Pdgfra* (oligodendrocyte precursor cell [OPC]), *Fyn* (newly formed oligodendrocyte [NFO]), and *Mobp* (myelinating oligodendrocyte [MO]) (Figures 2A and 2B). These subtypes reflect distinct stages of oligodendrocyte differentiation (Emery and Lu, 2015). The three *Sox9*$^+$ cell clusters could also be distinguished from one another by subtype markers *Agt* (astrocytes [Astro]), *Ccdc153* (ependymocyte [Ependy]), and *Rax* (tanycyte [Tany]) (Figures 2A and 2B). The two *Cldn5*$^+$ endothelial cell subtypes (Endo 1 and Endo 2) were marked by *Slc38a5* and *Myh11*, respectively (Figures 2A and 2B). The two *C1qa*$^+$ groups expressed either *Cx3cr1* or *Mrc1* (Figures 2A and 2B), representing microglia (Micro) and macrophages (Macro). The expression of some non-neuronal subtype markers in mouse hypothalamus is confirmed by ISH data from the Allen Brain Atlas (Figure 2C). Although the non-neuronal cell types identified here are similar to those found in other brain regions (Tasic et al., 2016; Zeisel et al., 2015), tanycytes, localizing in the ventral walls of the third ventricle (3V), were only identified in our dataset, demonstrating the power of our method in capturing region-specific cell types.

Oligodendrocyte Differentiation Is Associated with Dynamic Transcriptional Changes

Identifying OPC, NFO, and MO cell clusters in our dataset indicated that oligodendrocyte differentiation and axon myelination are still taking place in adult hypothalamus. Additionally, the single-cell transcriptomes of oligodendrocytes at different maturation stages provide an opportunity for understanding the transcriptional program of oligodendrocyte differentiation in vivo.

(C) Violin plot showing the expression of pan marker genes across the 45 cell clusters. Each cluster is color-coded. The mRNA level is shown on linear scale and adjusted for different genes. The maximum TPM value of each pan marker gene is presented on the right. *Snap25* and *Syt1*, pan-neuronal markers; *Slc17a6*, pan-glutamatergic marker; *Slc32a1*, pan-GABAergic marker; *Olig1*, *Sox9*, *Cldn5*, and *C1qa* each marks multiple non-neuronal clusters. Glu1–Glu15, glutamatergic neuron cluster 1–15; GABA1–GABA18, GABAergic neuron cluster 1–18; Hista, histaminergic neuron; NN1–NN11, non-neuron cluster 1–11.
(D) tSNE plots showing expression of pan marker genes in distinct cell clusters. The gene expression level is color-coded.
See also Figure S1.

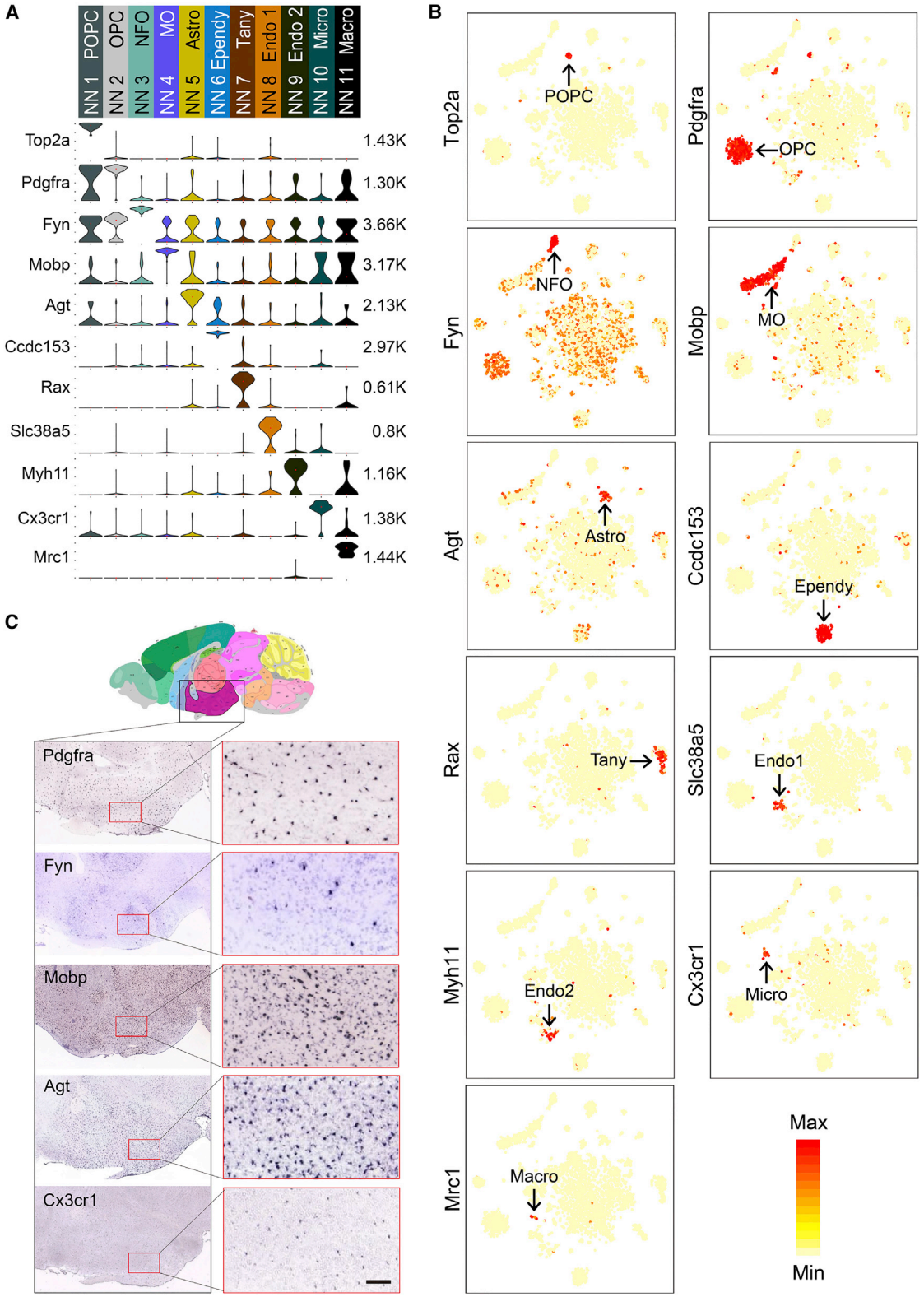

Figure 2. Overview of the 11 Non-neuronal Cell Clusters in Hypothalamus

(A) Violin plot showing the expression profile of representative marker genes in the 11 non-neuronal cell clusters. Different clusters are color-coded. The mRNA level is shown on a linear scale and adjusted for different genes. The maximum TPM value of each gene is presented on the right. POPC, proliferating

(legend continued on next page)

To this end, we performed an unsupervised pseudotime analysis with Monocle (Trapnell et al., 2014), in which OPCs, NFOs, and MOs were linked according to their gene expression profile (Figure 3A). Based on the established differentiation direction of oligodendrocyte (Emery and Lu, 2015), we chose the direction of OPCs to NFOs and then to MOs (Figure 3A). Sequential expression of *Pdgfra*, *Fyn*, and *Mog* matches this direction (Figure 3B), indicating that the pseudotime axis mimics the oligodendrocyte maturation process. To further characterize the transcriptional program underlying oligodendrocyte differentiation, we identified six groups of genes with distinct expression patterns along the differentiation process (Figures 3C and 3D; Table S2). Gene ontology (GO) analysis revealed that different biological processes were enriched in different gene groups (Table S3). For example, the genes in groups 1 and 2, which are highly expressed in OPCs but repressed during oligodendrocyte maturation, are enriched for regulation of development and differentiation, while genes in groups 5 and 6 with a low-to-high trend are enriched for axon ensheathment and myelination. Notably, genes in group 3 are high in NFOs, suggesting that these genes might be important for OPCs to MOs transition. Consistently, several genes of this group have been found to play a role in oligodendrocyte differentiation, such as *Bmp4* (Samanta and Kessler, 2004) and *Gpr17* (Chen et al., 2009) (Figure 3E). Interestingly, some epigenetic factors, such as *Sirt2* and *Dnmt3a*, are also highly transcribed in NFO (Figure 3E), indicating that chromatin remodeling and epigenetic regulation may play an important role during oligodendrocyte maturation.

A very recent study also analyzed mouse oligodendrocyte subtypes and differentiation using scRNA-seq (Marques et al., 2016). Using Drop-seq, a different scRNA-seq technique, we successfully captured the OPC to MO differentiation process in adult mouse hypothalamus through pseudotime analysis. Importantly, the transcriptional dynamics of stage-specific genes along the developmental axis revealed in our study is highly similar to the other study (Marques et al., 2016) (Figure S3), thus validating our approach.

ScRNA-Seq Reveals Transcriptional Features of Tanycyte and Tanycyte Subtypes

Tanycyte is a hypothalamus-specific non-neuronal cell type. The cell bodies of tanycytes occupy the floor and ventrolateral walls of the 3V and project laterally into adjacent hypothalamic regions, including dorsomedial hypothalamic nucleus (DMH), ventromedial hypothalamic nucleus (VMH), arcuate hypothalamic nucleus (ARH), and median eminence (ME) (Bolborea and Dale, 2013). This morphological feature distinguishes tanycytes from neighboring ependymocytes that occupy dorsal walls of the 3V (Goodman and Hajihosseini, 2015) (Figure 4A). Previous studies have revealed important functions of tanycytes in regulating energy homeostasis through diverse mechanisms (Goodman and Hajihosseini, 2015), but the underlying molecular mechanism remains largely unknown.

Our clustering analysis identified a *Rax*$^{+}$ tanycyte cell cluster (Miranda-Angulo et al., 2014), which is distinct from the *Ccdc153*$^{+}$ ependymocyte cluster (Figures 2A and 2B), indicating that tanycytes are transcriptionally distinct from ependymocytes and other cell types (Figure S4A). Consistent with previous studies (Lee et al., 2012; Robins et al., 2013), we found that the radial glia makers Nestin (*Nes*) and Vimentin (*Vim*) are highly transcribed in tanycytes (Figure S4B), suggesting that these cells may originate from embryonic radial glia and function as neural stem cells in adult hypothalamus (Lee et al., 2012). However, both *Nes* and *Vim* are also highly expressed in ependymal cells (Figure S4B) and as such cannot serve as tanycyte-specific markers. To characterize the molecular features of tanycytes and their neighboring ependymal cells, we compared the transcription profiles of these two cell clusters (Figure 4B), which revealed many genes that are differentially expressed in tanycytes and ependymocytes (Table S4). GO analysis of the tanycyte-specific genes identified terms that include signal transduction, GPCR signaling pathway, and modulation of synaptic transmission (Figure S4C), consistent with the known function of tanycytes in transmission of metabolic signals to neurons in regulating homeostasis (Goodman and Hajihosseini, 2015). The tanycyte-enriched genes include *Col23a1*, *Slc16a2*, *Lhx2*, and *Ptn* (Figures 4C and S4D), some of which have been linked to tanycyte development and function, such as *Lhx2* (Salvatierra et al., 2014) and *Slc16a2* (Mayerl et al., 2014). To test the potential of these differentially expressed genes to serve as tanycyte- and ependymocyte-specific markers, we examined their expression pattern in mouse brain with the ISH data from Allen Brain Atlas. Data shown in Figures 4C and S4D confirmed that these genes marked different cell populations along the dorsal-ventral axis of the 3V walls, which is consistent with the known location of tanycytes and ependymal cells (Figure 4A).

In addition to identifying tanycyte-specific markers, we further analyzed transcriptional heterogeneity among the tanycyte subtypes. Currently, tanycytes are separated into different subpopulations based on their physical location: dorsal tanycytes projecting to DMH and VMH are named α tanycytes, which are further divided into more dorsal α1 subtype and more ventral α2 subtype, the cells distributed at the ventral 3V walls that are in contact with ARH are termed β1 tanycytes, and the cells located at the bottom of the 3V walls that are in contact with ME are regarded as β2 tanycytes (Mathew, 2008). The lack of reliable molecular markers of tanycyte subtypes is a major hurdle preventing understanding tanycyte subtype-specific function. To overcome this hurdle, we attempted to identify tanycyte subtype markers by analyzing the scRNA-seq data of the tanycytes.

oligodendrocyte progenitor cell; OPC, oligodendrocyte progenitor cell; NFO, newly formed oligodendrocytes; MO, myelinating oligodendrocyte; Astro, astrocyte; Ependy, ependymocyte; Tany, tanycyte; Endo, endothelial cell; Micro, microglia; Macro, macrophage.

(B) tSNE plots showing the expression of representative marker genes are restricted to specific non-neuronal clusters among all of the cells. The expression level is color-coded.

(C) In situ hybridization (ISH) data from Allen Brain Atlas showing the expression of non-neuronal subtype markers *Pdgfra*, *Fyn*, *Mobp*, *Agt*, and *Cx3cr1* in hypothalamus. Left: the coronal sections of the entire hypothalamic region. Right: enlarged images of the regions in red squares. Scale bar, 100 μm.

See also Figure S2.

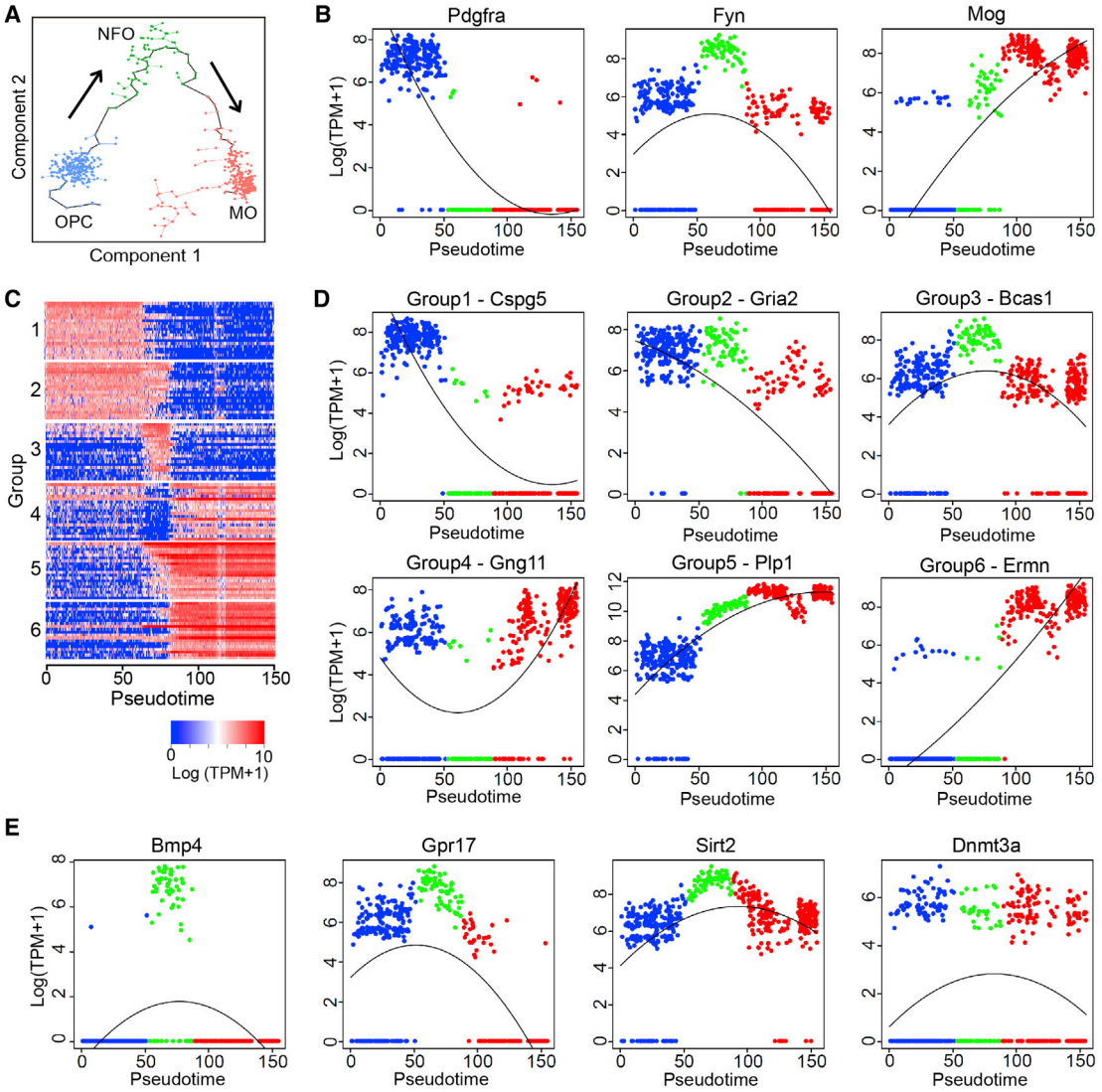

Figure 3. Transcriptional Dynamics during Oligodendrocyte Maturation

(A) Unsupervised ordering of OPCs (blue), NFOs (green), and MOs (red) based on their gene expression profiles. Minimal spanning tree is shown in black. Arrows indicate the direction of differentiation.

(B) Scatterplots showing the transcriptional dynamics of *Pdgfra*, *Fyn*, and *Mog* along the pseudotime. X axis represents the pseudotime axis, y axis shows gene expression level on log scale. Blue, green, and red dots represent OPCs, NFOs, and MOs, respectively.

(C) Heatmap showing six groups of genes with distinct expression dynamics during oligodendrocyte maturation. Columns are individual cells organized along the pseudotime and rows represent individual genes. Twenty of the most representative genes from each group are plotted. Expression level is color-coded.

(D) Scatterplots showing the transcriptional dynamics of representative genes belong to groups 1 to 6 in Figure 2C along the maturation of oligodendrocyte.

(E) Scatterplots showing the expression of NFO-specific genes *Bmp4*, *Grp17*, *Sirt2*, and *Dnmt3a* along the pseudo-timeline.

See also Figure S3.

We first identified highly variable genes within tanycyte cluster through principle components analysis (PCA). By plotting these genes on the tSNE map and comparing these with the public ISH dataset, we found a good correlation between the distribution pattern of the candidate marker genes on tSNE map and their in situ expression pattern along the ventral-dorsal axis (Figure 4D). For example, the *Slc17a8* and *Col25a1* located in the two most distal parts of the tSNE map are consistent with the ISH data showing that they are expressed in the most dorsal- and ventral-tanycyte cell populations, respectively (Figure 4D). Based on the tSNE map and ISH data, and considering the spatial distribution of tanycyte subtypes (Mathew, 2008), we believe that *Slc17a8* and *Col25a1* can serve as potential markers for α1 and β subtypes, respectively. Similarly, the expression patterns of other tanycyte subtype-specific genes can be predicted based on tSNE map (Figures 4D and S4E) and some of these are supported by ISH data (Figure 4D). Notably, although specific marker genes (or combinations of marker genes) can

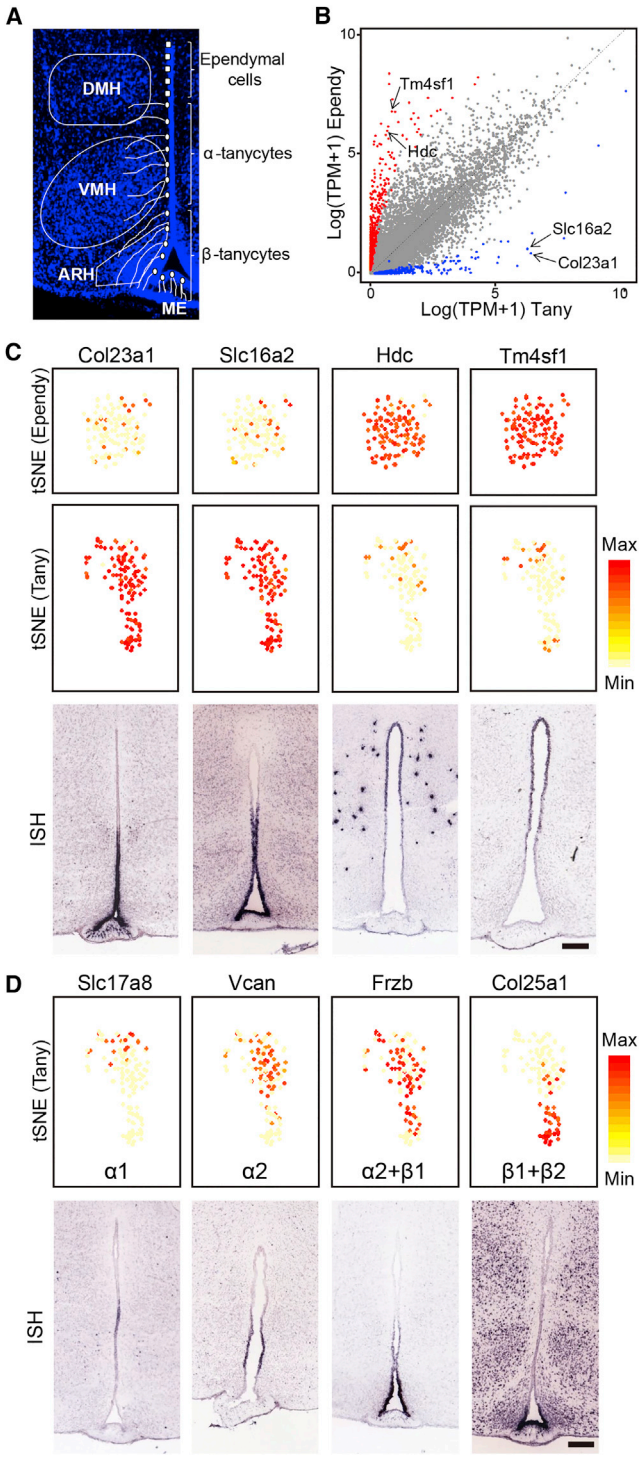

Figure 4. Gene Expression Features of Tanycyte and Tanycyte Subtypes

(A) Schematic diagram showing the spatial distribution and morphology of tanycytes, which can be further divided into α and β subtypes. ARH, arcuate hypothalamic nucleus; VHM, ventromedial hypothalamic nucleus; DMH, dorsomedial hypothalamic nucleus; ME, median eminence.

(B) Scatterplot comparing the expression profiles of tanycytes and ependymocytes. X axis and y axis represent the average expression level of certain genes among all tanycytes and all ependymal cells, respectively. Each dot represents a single gene, blue dots represent tanycyte-enriched genes and red dots represent ependymocyte-enriched genes. The tanycyte-specific genes *Col23a1* and *Slc16a2*, as well as the ependymocyte-specific genes *Hdc* and *Tm4sf1* are indicated by arrows.

(C) Expression patterns of selected tanycyte- and ependymocyte-specific genes. tSNE plots (upper and middle panels) showing the selective expression of *Col23a1* and *Slc16a2* in tanycytes (Tany), *Hdc* and *Tm4sf1* in ependymocytes (Ependy). Gene expression level is color-coded. ISH data (lower panels, from Allen Brain Atlas) show the distribution of corresponding genes along the 3V walls. Scale bar, 200 μm.

(D) Potential tanycyte subtype markers identified by scRNA-seq. tSNE plots (upper panels) showing the expression of selected genes enriched in subsets of tanycytes. The genes are ordered according to their expression level along the vertical axis of the tSNE map. For each gene, potential tanycyte subtype(s) that express the marker gene are listed. Gene expression level is color-coded. ISH data (lower panels, from Allen Brain Atlas) indicate a dorsal-to-ventral distribution of corresponding genes along the 3V walls. Scale bar, 200 μm. See also Figure S4.

be used to roughly separate tanycyte subtypes, many genes exhibited a gradient, rather than a clear-cut distribution across tanycyte subpopulations (Figures 4D and S4E), consistent with the notion that tanycytes may be composed of continuous cell trajectory with transition zones between different subtypes (Mathew, 2008).

The Hypothalamus Harbors Multiple Transcriptionally Distinct Neuron Subtypes

Our clustering analyses identified 15 glutamatergic neuron subtypes (Glu1–GLu15), 18 GABAergic neuron subtypes (GABA1–GABA18), and 1 histaminergic neuron cluster (Hista) expressing high levels of *Hdc* but negligible *Slc17a6* or *Slc32a1* (Figure 1C). We generated single-cell transcriptome heatmaps (Figure S5A) and visualized the glutamatergic and GABAergic neuron subtypes by tSNE (Figures 5A and 5B). In addition, potential subtype-specific marker genes for each of the 34 neuronal clusters were identified (Table S5). The majority of the 34 neuronal clusters contain subtype-specific genes that are unique to that cluster, and in some cases, a neuron cluster could be defined by the combinatorial expression of marker genes (Figures 5C and 5D). As expected, a number of neuron subtypes are distinguished by the expression of specific neuropeptides. For example, *Kiss1* and *Pomc* could represent Glu11 and Glu13 cell clusters, respectively (Figure 5C), while *Vip* and *Agrp* could represent GABA9 and GABA15 cell clusters, respectively (Figure 5D). Additionally, many transcription factors (e.g., *Foxb1* for Glu5, *Npas1* for GABA2, *Lhx8* for GABA5) exhibited neuron subtype-specific expression pattern (Figures 5C and 5D) consistent with their role in controlling neuron differentiation and identity.

Based on expression of the marker genes, many neuronal subtypes identified here could be assigned to neuron subtypes already described in the hypothalamus. For example, in glutamatergic clusters, Glu5 represents neurons in the mammillary body (MM) that express *Foxb1* (Figure S5B), while Glu11 and Glu13 represent *Kiss1*$^+$ and *Pomc*$^+$ neurons in ARH. On the other hand, the GABA8 and GABA9 clusters represent *Avp*$^+$ and *Vip*$^+$ neurons in the suprachiasmatic nucleus (SCH), while GABA11 and GABA15 clusters represent *Ghrh*$^+$ and *Agrp*$^+$ neurons in ARH. In addition to confirming known hypothalamic neuron

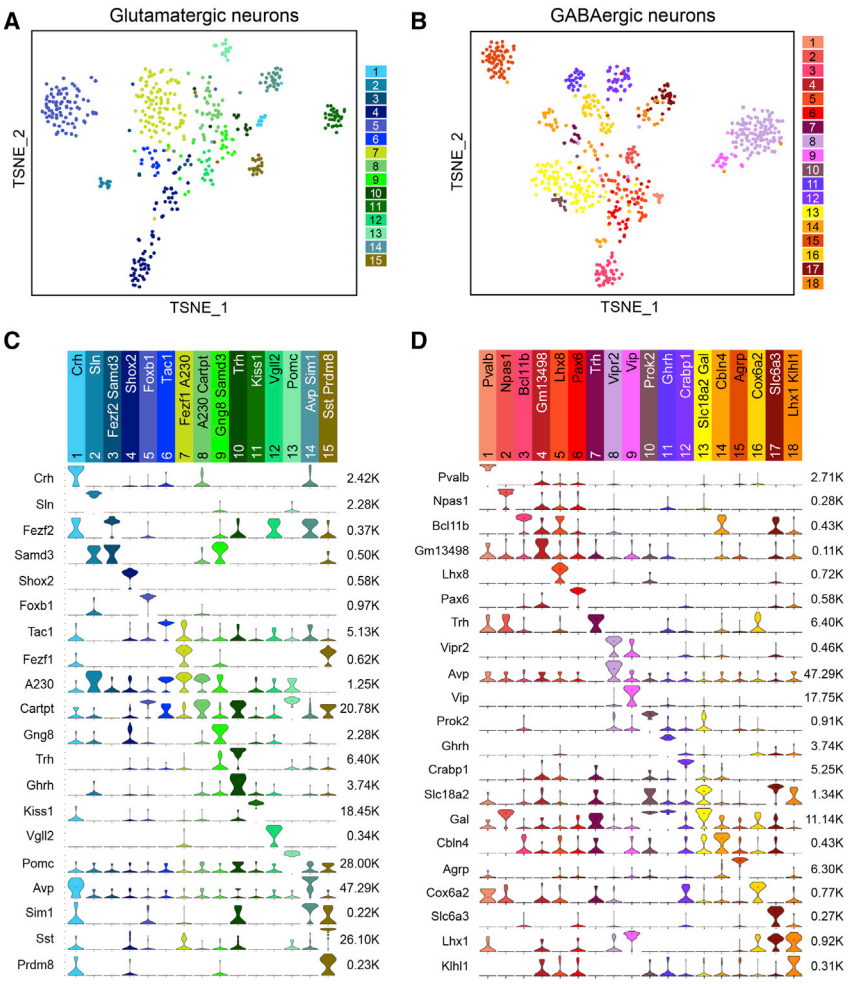

Figure 5. Glutamatergic and GABAergic Neuron Subtypes in Hypothalamus

(A) tSNE plot showing the 15 glutamatergic neuron subtypes identified in hypothalamus. Differentially expressed genes among all subtypes are used for dimension reduction. Different neuron subtypes are color-coded.

(B) tSNE plot showing the 18 GABAergic neuron subtypes in hypothalamus.

(C) Violin plots showing the expression of subtype markers across the 15 glutamatergic neuron subtypes. Columns represent different neuron clusters which are color-coded. Marker genes for each cluster are indicated. The gene expression level is shown on linear scale and adjusted for different genes. The maximum TPM value for each marker gene is presented on right. A230 is A230065H16Rik.

(D) Violin plots showing the expression of subtype markers across the 18 GABAergic neuron subtypes. Columns represent different neuron clusters which are color-coded.

See also Figure S5.

subtypes, our dataset also revealed gene expression features in specific neuron clusters. For example, *Cartpt* and *Cck* are actively transcribed in the Glu5 cluster (*Foxb1*$^{+}$ neuron in MM), while *Prph* and *Wif1* were co-expressed with *Hdc* in the Hista cluster (histaminergic neurons in tuberomammillary nucleus), both of which were verified by ISH (Figures S5B and S5C). Additionally, we found that the combined expression of *Sst* and *Prdm8* defines the *Sst*$^{+}$ neuroendocrine cells (Figure 5C, Glu15) located in PVpo (periventricular hypothalamic nucleus, preoptic part) with known function in regulating growth hormone secretion (Murray et al., 2015), but without a definitive molecular marker. We confirmed the co-expression of Sst and Prdm8 in PVpo, but not in cortex, by immunostaining (Figure S5D). Collectively, these results demonstrate that our unbiased scRNA-seq analyses are able to reveal cell types as well as cell-type-specific transcriptional features in the hypothalamus.

Relationship among Neuron Subtypes Assessed by Transcriptome

Currently, the developmental relationship among the different neuron subtypes in the hypothalamus is largely unknown. Taking advantage of the scRNA-seq dataset, we performed pairwise comparison and hierarchical clustering analyses on the glutamatergic and GABAergic neuron populations to assess their relationship based on transcriptome (Figure S5E). Interestingly, we found six glutamatergic clusters (Glu10 to Glu15), which represented different neurosecretory cells, are clustered together (Figure S5E). The separation of these neurons from the other glutamatergic subtypes indicates that these neurons possess distinct transcriptional programs that may reflect their distinct developmental process and functional properties. On the other hand, among GABAergic clusters, the SCH *Vipr2*$^{+}$ (GABA8) and *Vip*$^{+}$ (GABA9) neurons clustered together (Figure S5E), consistent with their similar developmental origin (VanDunk et al., 2011) and function (regulating circadian rhythm) (Dibner et al., 2010). These observations indicate that our cell-type-specific transcriptomic dataset has the potential to reveal lineage relationship and functional relevance among the various hypothalamic neurons.

Divergent Expression Patterns of Neuropeptides and Receptors across Neuronal Subtypes

The expression and function of various neuropeptides in the hypothalamus has been widely studied. However, a comprehensive expression profile of neuropeptide and receptors in the hypothalamic neurons is still unavailable. Thus, we assessed the expression profile of different neuropeptides and receptors in different hypothalamic neuron subtypes and found a highly divergent expression pattern among the various neuronal subtypes (Figures 6A and 6B and S6).

First, we found that the expression of the majority of neuropeptide genes is restricted to one or a few neuron subtypes. For example, *Kiss1*, *Pomc*, *Npvf*, *Vip*, and *Agrp* are each expressed in only one neuron subtype, while *Tac2*, *Cck*, *Sst*, and

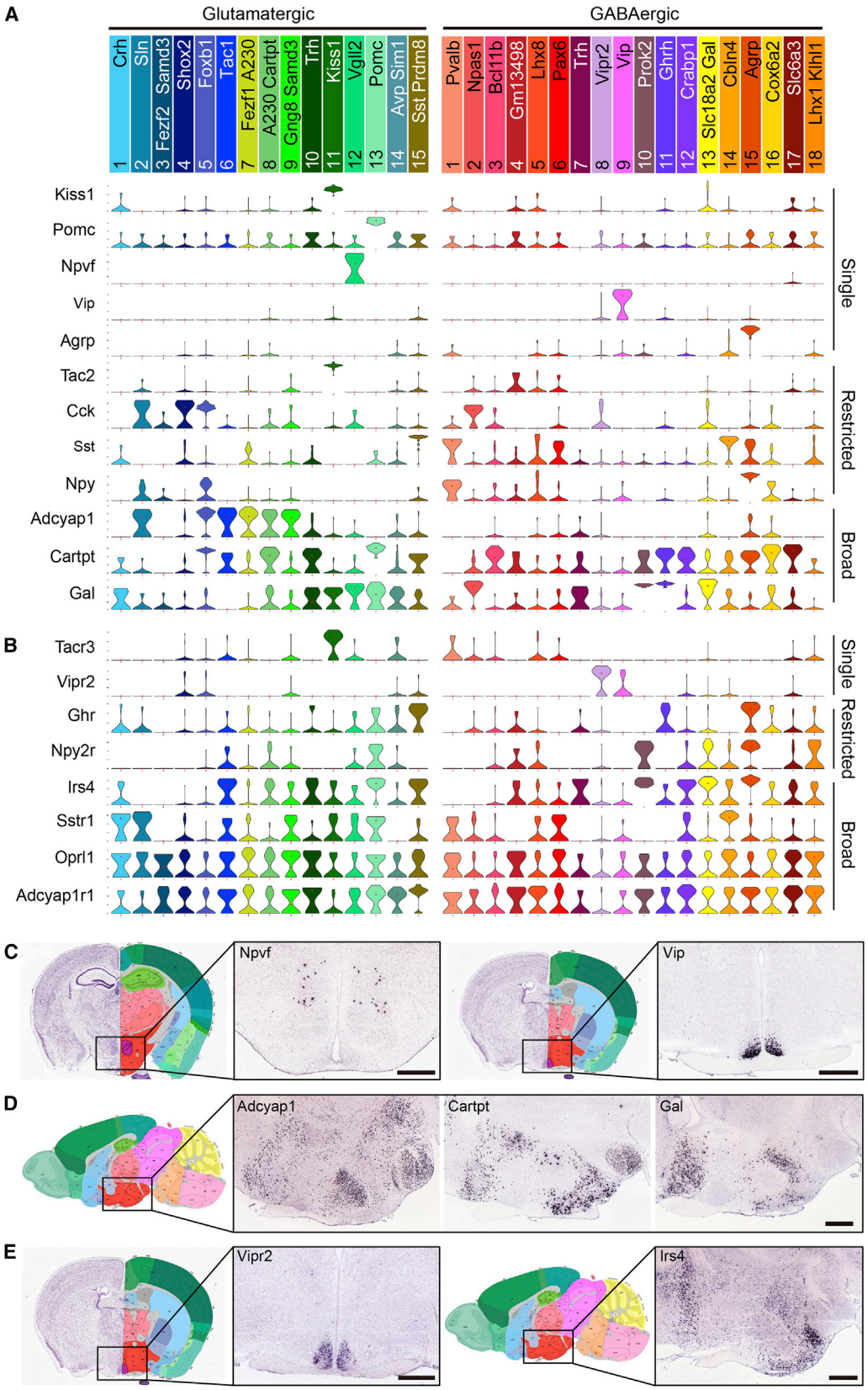

(legend on next page)

Npy are each expressed in two to four neuron subtypes with distinct patterns (Figures 6A and 6C). However, some neuropeptide genes, such as *Adcyap1*, *Cartpt*, and *Gal*, are expressed in multiple neuron subtypes (Figure 6A), consistent with their broad distribution in hypothalamus (Figure 6D). Although previous studies have used ISH or immunostaining to assess the co-expression of different neuropeptides, these methods can only profile a limited number of neuropeptides and neuron subtypes. Taking the advantage of our scRNA-seq dataset, we analyzed the gene expression profile of all detectable neuropeptides in the hypothalamic neuron subtypes. We found that co-expression of multiple neuropeptides is a common feature of many hypothalamic neurons. For instance, *Npy* is also expressed in *Agrp*$^+$ neurons (GABA15) and *Cartpt* is also expressed in *Pomc*$^+$ neurons (Glu13) (Figure 6A), which are consistent with previous findings (Schwartz et al., 2000). In addition, we found that *Sst*$^+$ neurons (GABA1) express *Npy*, while *Foxb1*$^+$ neurons (Glu5) co-express *Cck*, *Adcyap1*, and *Cartpt* (Figure 6A). Interestingly, *Ghrh* co-expresses with *Trh* in a glutamatergic population (Glu10) (Figure 5C), but also co-localizes with *Gal* in a GABAergic neuron subtype (GABA11) (Figure 5D). The extensive co-expression of multiple neuropeptide genes in a neuron subtype suggests complex crosstalk among different peptide signaling pathways.

Expression of a specific neuropeptide in certain neuron subtypes determines a specific signal that can be sent from these cells. Conversely, expression of a specific neuropeptide receptor indicates that these cells can receive a specific signal. Thus, we also analyzed the gene expression profiles of neuropeptide receptors among the various hypothalamic neuron subtypes. We found that like the expression profile of neuropeptides, the expression profile of neuropeptide receptors mRNA is also very diverse (Figures 6B and S6B). Some receptor genes are expressed in only one or a few neuron subtypes, such as *Vipr2* (GABA8) and *Ghr* (Glu15 and GABA15) (Figures 6B and 6E), which are consistent with previous studies (Harmar et al., 2002; Murray et al., 2015). In contrast, several peptide receptor genes, such as *Irs4*, *Sstr1*, *OPrl1*, and *Adcyap1r1*, are broadly expressed in multiple neuron subtypes (Figures 6B and 6E), suggesting extensive regulatory roles of these signaling pathways in the hypothalamus. Notably, a number of neuropeptide receptors genes are co-expressed with their ligands in some neuron subtypes, such as *Tacr3* in *Tac2*$^+$ neurons (Glu11), *Sstr1* in *Sst*$^+$ neurons (GABA1 and GABA14), and *Npy2r* in *Npy*$^+$ neurons (GABA15) (Figures 6A and 6B), indicating that a feedback mechanism may be used to regulate the corresponding neuropeptide secretion in these neuron subtypes.

Earlier studies on peptidergic neuron function in hypothalamus have paid less attention to the role of fast synaptic transmission mediated by conventional neurotransmitters. However, the potential interactions between slow-acting peptidergic signals and fast ionotropic signals are supported by some recent studies, which suggest an essential role of GABA/glutamate-mediated synaptic transmission in controlling animal behaviors in certain peptidergic neurons (Krashes et al., 2014; Tong et al., 2008). Consistently, our dataset shows that all hypothalamic peptidergic neurons can be categorized into either glutamatergic (*Slc17a6*$^+$) or GABAergic (*Slc32a1*$^+$) (Figure 6A), indicating that most, if not all, peptidergic neurons could communicate with downstream targets through fast synaptic transmission. Notably, the neurotransmitter and neuropeptide present in the same neuron do not necessarily function simultaneously because they are packed into different types of vesicles and respond to distinct neuronal activity (Ludwig and Leng, 2006).

Collectively, our data provide a comprehensive neuropeptide and receptor expression profile of hypothalamic neuron subtypes, which suggests complex crosstalk among the different neuropeptide signaling pathways, between neuropeptides and neurotransmitters, and between different peptidergic neuron populations.

Neuronal Subtypes Revealed by Single Cell RNA-Seq

Unbiased scRNA-seq is capable of de novo discovery of cell types with distinct transcriptional features. Indeed, we identified several neuronal subtypes with specific molecular markers from our dataset. For instance, we found that *Crabp1*, which encodes a retinoic acid binding protein, is highly expressed in the GABA12 cluster (Figure 7A). ISH and immunostaining showed that this gene is restricted to the ARH across the hypothalamus (Figure 7B), suggesting that it marks a distinct neuronal subtype in this region. To exclude the possibility that *Crabp1* is expressed from other known cell populations located in ARH, we queried the expression of *Kiss1*, *Pomc*, *Ghrh*, *Th*, and *Agrp* in *Crabp1*$^+$ neurons. All of them are highly expressed in specific cell types in ARH (Figure 7A). Our data showed that none of these genes are expressed in *Crabp1*$^+$ neurons (Figure 7A), supporting the notion that the *Crabp1*$^+$ neurons represent a cell type in ARH. Another neuron subtype identified in our study is the *Pax6*$^+$ GABAergic neuron (GABA6). Pax6 has an established function in neural development (Ypsilanti and Rubenstein, 2016), but its expression profile and function in the adult brain is largely unknown. A recent study has identified a *Pax6*$^+$ interneuron population in layer I of cerebral cortex (Zeisel et al., 2015). Here, we found that *Pax6* is specifically expressed in the GABA6 cluster (Figure 5D). Both ISH and antibody staining support the

Figure 6. Divergent Expression Pattern of Neuropeptides and Receptors among the Hypothalamic Neuron Subtypes

(A) Violin plots showing the expression of selected neuropeptides among the neuron subtypes in hypothalamus. Gene expression level is presented on linear scale and adjusted for different genes.

(B) Violin plots showing the expression of selected neuropeptide receptors among the neuron subtypes in hypothalamus.

(C) Coronal sections showing that *Npvf* and *Vip* are selectively expressed in different hypothalamic regions. ISH data are from Allen Brain Atlas. The boxed regions in the left panels were enlarged and shown in right panels.

(D) Sagittal sections showing the broad distribution of *Adcyap1*, *Cartpt*, and *Gal* in hypothalamus.

(E) ISH showing that *Vipr2* is selectively expressed in superchiasmatic nucleus while *Irs4* is widely distributed in hypothalamus.

Scale bars, 500 μm. See also Figure S6.

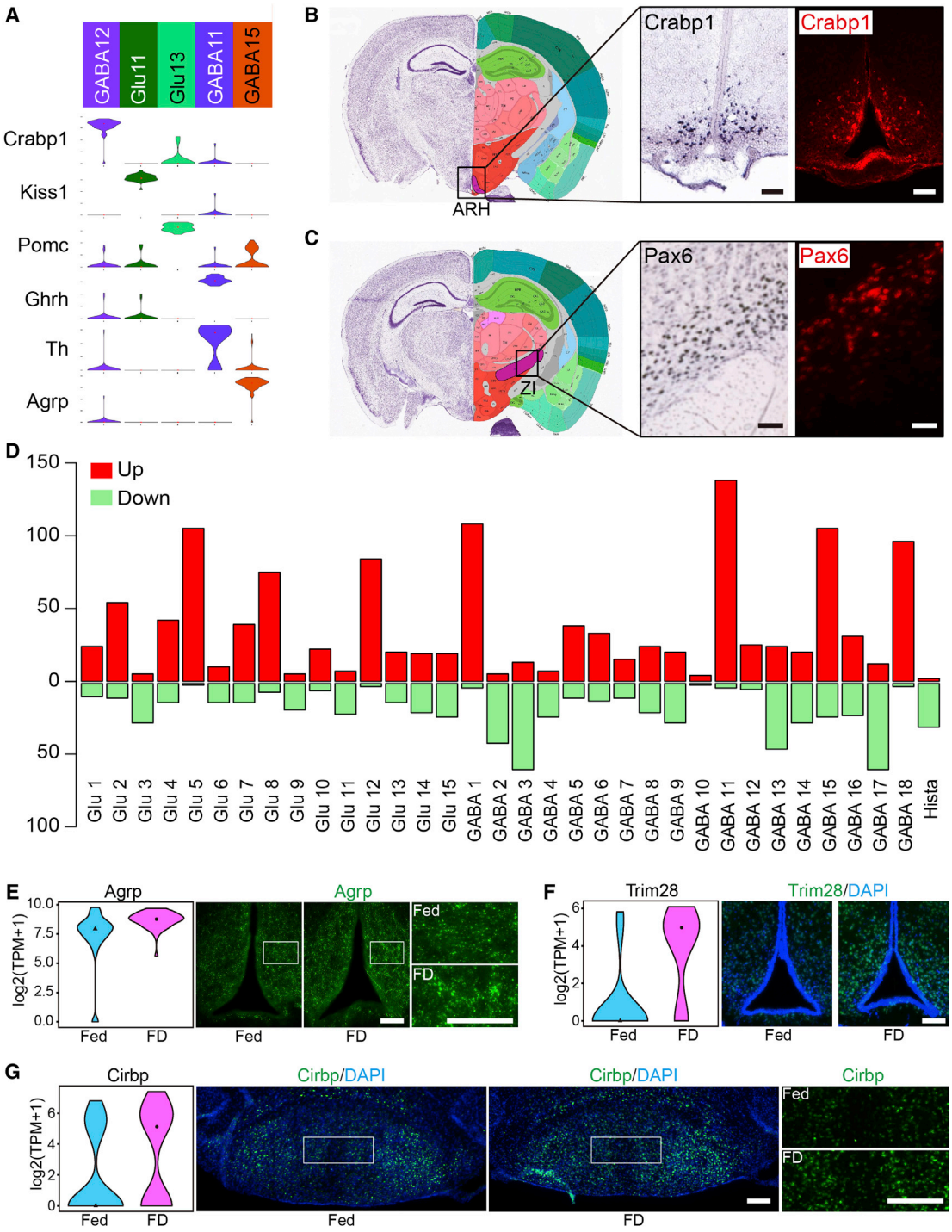

Figure 7. Neuron Types and Assessment of Food Deprivation-Induced Transcriptional Changes in Hypothalamus

(A) Violin plot showing the expression of selected genes in neuron subtypes located in ARH. Gene expression level is shown on linear scale and adjusted for different genes.

(B) ISH and immunostaining on coronal hypothalamus sections showing that the *Crabp1*$^{+}$ neurons are restricted in ARH. ISH data are from Allen Brain Atlas. Scale bars, 100 μm.

(C) ISH and immunostaining showing presence of *Pax6*$^{+}$ neurons in ZI. Scale bars, 100 μm.

(D) Bar graphs showing the number of genes affected by food deprivation across hypothalamic neuron subtypes. Red and green bars represent up- and downregulated genes. See also Table S6.

(legend continued on next page)

localization of *Pax6*$^+$ neurons in the zona incerta (ZI) (Figure 7C), a hypothalamic region whose cell composition and function are poorly understood. Identifying *Crabp1*$^+$ and *Pax6*$^+$ neuronal subtypes in the hypothalamus has set the stage for dissecting their specific functions in the hypothalamus.

Cell-Type-Specific Transcriptional Response to Food Deprivation Revealed by scRNA-Seq

Hypothalamus is an important brain region controlling feeding and metabolism (Schwartz et al., 2000). Classification of the various neuronal subtypes allows us to identify the neuron subtypes involved in regulating feeding behavior. To this end, we examined the transcriptional response to food deprivation across the hypothalamic neuronal subtypes by comparing single-cell gene expression profiles between ad libitum fed and food-deprived mice. The results revealed that food deprivation has differential effects on gene expression of the various hypothalamic neuron subtypes. The differentially expressed genes (DEGs) are mainly enriched in Glu5, Glu8, Glu12, GABA1, GABA11, GABA15, and GABA18 clusters (Figures 7D and S7A; Table S6), indicating that these neuronal subtypes are the main cells responding to food deprivation. Identification of the *Agrp*$^+$ (GABA15), *Ghrh*$^+$ (GABA11), and *Npvf*$^+$ (Glu12) neurons as food deprivation-responding cell types are consistent with previous studies (Henry et al., 2015; Murray et al., 2015; Wahab et al., 2015) and thus validate our approach. Importantly, scRNA-seq uncovered cell types, such as MM neurons (Glu5), that were not previously linked to energy homeostasis, exemplifying the ability of our unbiased approach in revealing neuron subtype-specific functions. GO analyses showed that DEGs identified in different neuronal clusters are enriched for genes of distinct functions (Figure S7B; Table S7) indicating that different neuronal subtypes are functionally different. To confirm the gene expression changes revealed by scRNA-seq, we first focused on *Agrp*$^+$ neurons (GABA15), which are known for controlling feeding and energy expedition. Immunostaining showed that the Agrp level was significantly increased upon food deprivation (Figure 7E), consistent with our scRNA-seq result and previous knowledge (Henry et al., 2015). Additionally, immunostaining confirmed upregulation of Trim28 in *Ghrh*$^+$ neurons (GABA11) in the ARH and increased expression of Cirbp in MM neurons (Glu5) upon food deprivation (Figures 7F and 7G).

DISCUSSION

Comprehensive Cell-Type Classification in Hypothalamus Can Facilitate Its Functional Study

Understanding the cell composition and cell-type-specific transcription features of the hypothalamus is essential for understanding the function of this important brain region. Several previous studies have attempted to characterize the cell types in the hypothalamus based on cell location, morphology, connection, function, and marker gene expression (Brown et al., 2013; Lee et al., 2015; Mathew, 2008; Wu et al., 2014). However, a systematic hypothalamic cell map of transcriptomic features is still lacking. Using the Drop-seq technique (Macosko et al., 2015), we profiled transcriptomes of more than 14,000 single cells and identified 45 transcriptionally distinct cell subtypes in the adult mouse hypothalamus. Most of the non-neuronal cell types identified in this study are similar to those found in the cerebral cortex (Zeisel et al., 2015), suggesting that most non-neuronal cells are widely distributed across various brain regions. In contrast, the neuronal cell types are largely hypothalamus-specific, indicating that different neuron composition underlies distinct functions of different brain regions. Our work, therefore, provides a comprehensive overview of hypothalamic cell types based on their transcriptional features, which will greatly facilitate functional studies of hypothalamus.

First, the cell-type-specific markers identified here provide an unambiguous cell-type definition, which can help to unify studies from different laboratories to resolve confusion generated due to the use of different criteria in defining cell types. Second, the information of unique and combinatorial markers for different cell types enable the development of genetic or viral tools to achieve cell-type-specific labeling and manipulation, which is essential for dissecting cell-type-specific function in such a complex brain region. Third, by assessing the relationship of different hypothalamic cell types based on transcriptional profiles, hypotheses regarding the development and function of different cell subtypes can be generated and tested, which in turn can advance our understanding of hypothalamus. Fourth, identifying *Crabp1*$^+$ neurons in ARH and *Pax6*$^+$ neurons in ZI indicates that uncharacterized neuron subtypes in hypothalamus still remain, even within a relatively well-studied region such as the ARH.

Divergent Expression Pattern of Neuropeptides and Receptors in the Hypothalamus

Understanding the expression and function of various neuropeptides has long been an interest of the hypothalamus scientific community. Our scRNA-seq datasets provide a comprehensive expression profile of neuropeptides and their receptors across hypothalamic neuron subtypes. Analysis of this expression profile has revealed several important features. First, neuropeptides feature a very divergent expression pattern and that cellular heterogeneity can be largely resolved based on the expression of a specific neuropeptide or a combination of neuropeptides. Second, co-expression of multiple neuropeptides can be analyzed in our dataset, thus facilitating the study of crosstalk among different neuropeptide signals. Third, by examining the distribution of neuropeptides and corresponding receptors, the

(E) Violin plots and immunostaining showing that Agrp is upregulated by food deprivation. Fed, n = 62; FD, n = 50. Fold change = 1.52, p = 0.00016. Fed, normal feeding; FD, food deprivation. Scale bars, 100 μm.
(F) Violin plots and immunostaining showing that Trim28 is upregulated in ARH by food deprivation. Fed, n = 16; FD, n = 19. Fold change = 2.76, p = 0.00081. Scale bar, 100 μm.
(G) Violin plot and immunostaining showing that Cirbp in MM neurons is upregulated by food deprivation. Fed, n = 103; FD, n = 97. Fold change = 1.97, p = 0.00099. Scale bars, 200 μm.
See also Figure S7.

potential regulatory relationship within individual neuron subtypes or among different neuron populations can be analyzed, revealing complex intra- or inter-population regulation. Fourth, our analysis has uncovered extensive overlap between neuropeptide and conventional neurotransmitters across hypothalamic neuron subtypes, indicating a functional interaction between the two neuronal signaling systems, which begs for further studies on the crosstalk between the slow peptidergic signaling and the fast ionotropic signaling.

Gene Expression Features of Tanycyte and Tanycyte Subtypes

Tanycyte is a hypothalamus-specific, non-neuronal cell type. Accumulating evidence suggests its diverse physiological functions in neuroendocrine, metabolism, and neurogenesis (Goodman and Hajihosseini, 2015). However, the molecular features underlying tanycyte heterogeneity and diverse function have been elusive. Our scRNA-seq dataset not only confirm tanycyte as a distinct cell type, but also reveal tanycyte-specific markers that can be used to distinguish them from ependymal cells. More importantly, by analyzing single-cell transcriptomes of tanycytes, we identified tanycyte subtypes with distinct transcription profiles. The tanycyte- and tanycyte-subtype-specific marker genes identified will allow the development of genetic tools for achieving cell-(sub)type-specific manipulation for dissection the function of tanycyte and tanycyte subtypes.

Revealing Cell-Type-Specific Transcriptional Response to Food Deprivation

In addition to cell-type classification, scRNA-seq can be applied to dissect cell-type-specific transcriptional dynamics in complex tissues under different physiological and pathological conditions. This is particularly important for the nervous system that has great cell heterogeneity and cell-subtype-specific functions (Knight et al., 2012), but conventional RNA-seq cannot resolve such level of cell-type heterogeneity. As a proof-of-principle study, we compared the transcriptional program between normal-fed and food-deprived animals across hypothalamic neuronal subtypes, which revealed 7 out of the 34 subtypes exhibit significant transcriptome changes. The analysis not only revealed the specific neuronal clusters that respond to food deprivation, but also uncovered cell types that have not been previously linked to feeding and energy homeostasis, thus highlighting the capability of unbiased single-cell profiling in revealing biological insight into brain functions.

EXPERIMENTAL PROCEDURES

Animals

All animal experiments followed the guidelines of the Institutional Animal Care and Use Committee at Harvard Medical School. Young adult female (8- to 10-week-old) B6D2F1 mice (C57B6 female × DBA2 male) were used. One day before the experiments, each animal was separated into individual fresh cages. For 24 hr food deprivation treatment, only water was provided.

Tissue Dissection, Single-Cell Dissociation, and Library Construction

The hypothalamus tissue was dissected from acute brain slices of adult (8- to 10-week-old) mice. The tissue was dissociated into single-cell suspension using a papain-based dissociation protocol (Brewer and Torricelli, 2007) with some modifications (see the Supplemental Experimental Procedures). The single cells and barcoded-beads were captured into nanoliter-sized droplets with microfluidic device, followed by library construction as previously described (Macosko et al., 2015).

Cell Clustering

The 3,319 cells with at least 2,000 genes detected in each single cell were used for clustering analysis. To classify the cells, the R package Seurat was used (Macosko et al., 2015). The highly variable genes were identified from these cells using Seurat with the default setting. Then these highly variable genes were used for principle component analysis (PCA). The statistically significant PCs were used for two-dimension t-distributed stochastic neighbor embedding (tSNE). Based on the tSNE map, density-based clustering (DBSCAN) was used to cluster cells based on their proximity, resulting in 40 clusters. The largest neuronal cluster containing 1,574 cells was extracted for further clustering using the same strategy described above. The same analysis was repeated for another two rounds. In total, 73 cell clusters were identified. Following this unsupervised clustering analysis, we further filtered out clusters representing double droplets, clusters from non-hypothalamic tissues, as well as clusters with less than ten cells (see the Supplemental Experimental Procedures). After filtering, a total of 45 cell clusters were identified.

ACCESSION NUMBERS

The accession number for the sequencing data reported in this work is GEO: GSE87544.

SUPPLEMENTAL INFORMATION

Supplemental Information includes Supplemental Experimental Procedures, seven figures, and seven tables and can be found with this article online at http://dx.doi.org/10.1016/j.celrep.2017.03.004.

AUTHOR CONTRIBUTIONS

Y.Z. and R.C. conceived the project. Y.Z. and R.C. designed the study. R.C. and X.W. performed the experiments. L.J. and X.W. analyzed the data. R.C., X.W., L.J., and Y.Z. interpreted the data. R.C. and Y.Z. wrote the manuscript.

ACKNOWLEDGMENTS

We thank Drs. Li Shen and Hao Wu for their initial help in establishing the Drop-seq platform, Dr. Sarah E. Ross for the Prdm8 antibody, and Dr. Luis M. Tuesta for critical reading of the manuscript. This project was partly supported by NIH U01 MH105960 and HHMI. Y.Z. is an investigator of the Howard Hughes Medical Institute.

Received: November 28, 2016
Revised: January 31, 2017
Accepted: February 28, 2017
Published: March 28, 2017

REFERENCES

Bolborea, M., and Dale, N. (2013). Hypothalamic tanycytes: potential roles in the control of feeding and energy balance. Trends Neurosci. *36*, 91–100.

Brewer, G.J., and Torricelli, J.R. (2007). Isolation and culture of adult neurons and neurospheres. Nat. Protoc. *2*, 1490–1498.

Brown, C.H., Bains, J.S., Ludwig, M., and Stern, J.E. (2013). Physiological regulation of magnocellular neurosecretory cell activity: integration of intrinsic, local and afferent mechanisms. J. Neuroendocrinol. *25*, 678–710.

Chen, Y., Wu, H., Wang, S., Koito, H., Li, J., Ye, F., Hoang, J., Escobar, S.S., Gow, A., Arnett, H.A., et al. (2009). The oligodendrocyte-specific G protein-coupled receptor GPR17 is a cell-intrinsic timer of myelination. Nat. Neurosci. *12*, 1398–1406.

Denton, D.A., McKinley, M.J., and Weisinger, R.S. (1996). Hypothalamic integration of body fluid regulation. Proc. Natl. Acad. Sci. USA *93*, 7397–7404.

Dibner, C., Schibler, U., and Albrecht, U. (2010). The mammalian circadian timing system: organization and coordination of central and peripheral clocks. Annu. Rev. Physiol. *72*, 517–549.

Elmquist, J.K., Elias, C.F., and Saper, C.B. (1999). From lesions to leptin: hypothalamic control of food intake and body weight. Neuron *22*, 221–232.

Emery, B., and Lu, Q.R. (2015). Transcriptional and epigenetic regulation of oligodendrocyte development and myelination in the central nervous system. Cold Spring Harb. Perspect. Biol. *7*, a020461.

Gokce, O., Stanley, G.M., Treutlein, B., Neff, N.F., Camp, J.G., Malenka, R.C., Rothwell, P.E., Fuccillo, M.V., Südhof, T.C., and Quake, S.R. (2016). Cellular taxonomy of the mouse striatum as revealed by single-cell RNA-seq. Cell Rep. *16*, 1126–1137.

Gong, S., Zheng, C., Doughty, M.L., Losos, K., Didkovsky, N., Schambra, U.B., Nowak, N.J., Joyner, A., Leblanc, G., Hatten, M.E., and Heintz, N. (2003). A gene expression atlas of the central nervous system based on bacterial artificial chromosomes. Nature *425*, 917–925.

Goodman, T., and Hajihosseini, M.K. (2015). Hypothalamic tanycytes-masters and servants of metabolic, neuroendocrine, and neurogenic functions. Front. Neurosci. *9*, 387.

Greig, L.C., Woodworth, M.B., Galazo, M.J., Padmanabhan, H., and Macklis, J.D. (2013). Molecular logic of neocortical projection neuron specification, development and diversity. Nat. Rev. Neurosci. *14*, 755–769.

Harmar, A.J., Marston, H.M., Shen, S., Spratt, C., West, K.M., Sheward, W.J., Morrison, C.F., Dorin, J.R., Piggins, H.D., Reubi, J.C., et al. (2002). The VPAC(2) receptor is essential for circadian function in the mouse suprachiasmatic nuclei. Cell *109*, 497–508.

Henry, F.E., Sugino, K., Tozer, A., Branco, T., and Sternson, S.M. (2015). Cell type-specific transcriptomics of hypothalamic energy-sensing neuron responses to weight-loss. eLife *4*. http://dx.doi.org/10.7554/eLife.09800.

Jiang, X., Shen, S., Cadwell, C.R., Berens, P., Sinz, F., Ecker, A.S., Patel, S., and Tolias, A.S. (2015). Principles of connectivity among morphologically defined cell types in adult neocortex. Science *350*, aac9462.

Kiselev, V.Y., Kirschner, K., Schaub, M.T., Andrews, T., Yiu, A., Chandra, T., Natarajan, K.N., Reik, W., Barahona, M., Green, A.R., and Hemberg, M. (2016). SC3 - consensus clustering of single-cell RNA-seq data. bioRxiv *036558*. http://dx.doi.org/10.1101/036558.

Klein, A.M., Mazutis, L., Akartuna, I., Tallapragada, N., Veres, A., Li, V., Peshkin, L., Weitz, D.A., and Kirschner, M.W. (2015). Droplet barcoding for single-cell transcriptomics applied to embryonic stem cells. Cell *161*, 1187–1201.

Knight, Z.A., Tan, K., Birsoy, K., Schmidt, S., Garrison, J.L., Wysocki, R.W., Emiliano, A., Ekstrand, M.I., and Friedman, J.M. (2012). Molecular profiling of activated neurons by phosphorylated ribosome capture. Cell *151*, 1126–1137.

Krashes, M.J., Shah, B.P., Madara, J.C., Olson, D.P., Strochlic, D.E., Garfield, A.S., Vong, L., Pei, H., Watabe-Uchida, M., Uchida, N., et al. (2014). An excitatory paraventricular nucleus to AgRP neuron circuit that drives hunger. Nature *507*, 238–242.

Lake, B.B., Ai, R., Kaeser, G.E., Salathia, N.S., Yung, Y.C., Liu, R., Wildberg, A., Gao, D., Fung, H.L., Chen, S., et al. (2016). Neuronal subtypes and diversity revealed by single-nucleus RNA sequencing of the human brain. Science *352*, 1586–1590.

Lee, D.A., Bedont, J.L., Pak, T., Wang, H., Song, J., Miranda-Angulo, A., Takiar, V., Charubhumi, V., Balordi, F., Takebayashi, H., et al. (2012). Tanycytes of the hypothalamic median eminence form a diet-responsive neurogenic niche. Nat. Neurosci. *15*, 700–702.

Lee, I.T., Chang, A.S., Manandhar, M., Shan, Y., Fan, J., Izumo, M., Ikeda, Y., Motoike, T., Dixon, S., Seinfeld, J.E., et al. (2015). Neuromedin s-producing neurons act as essential pacemakers in the suprachiasmatic nucleus to couple clock neurons and dictate circadian rhythms. Neuron *85*, 1086–1102.

Lein, E.S., Hawrylycz, M.J., Ao, N., Ayres, M., Bensinger, A., Bernard, A., Boe, A.F., Boguski, M.S., Brockway, K.S., Byrnes, E.J., et al. (2007). Genome-wide atlas of gene expression in the adult mouse brain. Nature *445*, 168–176.

Ludwig, M., and Leng, G. (2006). Dendritic peptide release and peptide-dependent behaviours. Nat. Rev. Neurosci. *7*, 126–136.

Macosko, E.Z., Basu, A., Satija, R., Nemesh, J., Shekhar, K., Goldman, M., Tirosh, I., Bialas, A.R., Kamitaki, N., Martersteck, E.M., et al. (2015). Highly parallel genome-wide expression profiling of individual cells using nanoliter droplets. Cell *161*, 1202–1214.

Marques, S., Zeisel, A., Codeluppi, S., van Bruggen, D., Mendanha Falcão, A., Xiao, L., Li, H., Häring, M., Hochgerner, H., Romanov, R.A., et al. (2016). Oligodendrocyte heterogeneity in the mouse juvenile and adult central nervous system. Science *352*, 1326–1329.

Mathew, T.C. (2008). Regional analysis of the ependyma of the third ventricle of rat by light and electron microscopy. Anat. Histol. Embryol. *37*, 9–18.

Mayerl, S., Müller, J., Bauer, R., Richert, S., Kassmann, C.M., Darras, V.M., Buder, K., Boelen, A., Visser, T.J., and Heuer, H. (2014). Transporters MCT8 and OATP1C1 maintain murine brain thyroid hormone homeostasis. J. Clin. Invest. *124*, 1987–1999.

Miranda-Angulo, A.L., Byerly, M.S., Mesa, J., Wang, H., and Blackshaw, S. (2014). Rax regulates hypothalamic tanycyte differentiation and barrier function in mice. J. Comp. Neurol. *522*, 876–899.

Murray, P.G., Higham, C.E., and Clayton, P.E. (2015). 60 YEARS OF NEUROENDOCRINOLOGY: The hypothalamo-GH axis: the past 60 years. J. Endocrinol. *226*, T123–T140.

Navarro, V.M., and Tena-Sempere, M. (2011). Neuroendocrine control by kisspeptins: role in metabolic regulation of fertility. Nat. Rev. Endocrinol. *8*, 40–53.

Puelles, L., and Rubenstein, J.L. (2015). A new scenario of hypothalamic organization: rationale of new hypotheses introduced in the updated prosomeric model. Front. Neuroanat. *9*, 27.

Robins, S.C., Stewart, I., McNay, D.E., Taylor, V., Giachino, C., Goetz, M., Ninkovic, J., Briancon, N., Maratos-Flier, E., Flier, J.S., et al. (2013). α-Tanycytes of the adult hypothalamic third ventricle include distinct populations of FGF-responsive neural progenitors. Nat. Commun. *4*, 2049.

Salvatierra, J., Lee, D.A., Zibetti, C., Duran-Moreno, M., Yoo, S., Newman, E.A., Wang, H., Bedont, J.L., de Melo, J., Miranda-Angulo, A.L., et al. (2014). The LIM homeodomain factor Lhx2 is required for hypothalamic tanycyte specification and differentiation. J. Neurosci. *34*, 16809–16820.

Samanta, J., and Kessler, J.A. (2004). Interactions between ID and OLIG proteins mediate the inhibitory effects of BMP4 on oligodendroglial differentiation. Development *131*, 4131–4142.

Schwartz, M.W., Woods, S.C., Porte, D., Jr., Seeley, R.J., and Baskin, D.G. (2000). Central nervous system control of food intake. Nature *404*, 661–671.

Shimogori, T., Lee, D.A., Miranda-Angulo, A., Yang, Y., Wang, H., Jiang, L., Yoshida, A.C., Kataoka, A., Mashiko, H., Avetisyan, M., et al. (2010). A genomic atlas of mouse hypothalamic development. Nat. Neurosci. *13*, 767–775.

Tasic, B., Menon, V., Nguyen, T.N., Kim, T.K., Jarsky, T., Yao, Z., Levi, B., Gray, L.T., Sorensen, S.A., Dolbeare, T., et al. (2016). Adult mouse cortical cell taxonomy revealed by single cell transcriptomics. Nat. Neurosci. *19*, 335–346.

Toledo-Rodriguez, M., Blumenfeld, B., Wu, C., Luo, J., Attali, B., Goodman, P., and Markram, H. (2004). Correlation maps allow neuronal electrical properties to be predicted from single-cell gene expression profiles in rat neocortex. Cereb. Cortex *14*, 1310–1327.

Tong, Q., Ye, C.P., Jones, J.E., Elmquist, J.K., and Lowell, B.B. (2008). Synaptic release of GABA by AgRP neurons is required for normal regulation of energy balance. Nat. Neurosci. *11*, 998–1000.

Trapnell, C., Cacchiarelli, D., Grimsby, J., Pokharel, P., Li, S., Morse, M., Lennon, N.J., Livak, K.J., Mikkelsen, T.S., and Rinn, J.L. (2014). The dynamics and regulators of cell fate decisions are revealed by pseudotemporal ordering of single cells. Nat. Biotechnol. *32*, 381–386.

VanDunk, C., Hunter, L.A., and Gray, P.A. (2011). Development, maturation, and necessity of transcription factors in the mouse suprachiasmatic nucleus. J. Neurosci. *31*, 6457–6467.

Wahab, F., Shahab, M., and Behr, R. (2015). The involvement of gonadotropin inhibitory hormone and kisspeptin in the metabolic regulation of reproduction. J. Endocrinol. *225*, R49–R66.

Wu, Z., Autry, A.E., Bergan, J.F., Watabe-Uchida, M., and Dulac, C.G. (2014). Galanin neurons in the medial preoptic area govern parental behaviour. Nature *509*, 325–330.

Ypsilanti, A.R., and Rubenstein, J.L. (2016). Transcriptional and epigenetic mechanisms of early cortical development: An examination of how Pax6 coordinates cortical development. J. Comp. Neurol. *524*, 609–629.

Zeisel, A., Muñoz-Manchado, A.B., Codeluppi, S., Lönnerberg, P., La Manno, G., Juréus, A., Marques, S., Munguba, H., He, L., Betsholtz, C., et al. (2015). Brain structure. Cell types in the mouse cortex and hippocampus revealed by single-cell RNA-seq. Science *347*, 1138–1142.

Cell Reports, Volume *18*

Supplemental Information

Single-Cell RNA-Seq Reveals Hypothalamic Cell Diversity

Renchao Chen, Xiaoji Wu, Lan Jiang, and Yi Zhang

Supplemental Figures

Figure S1

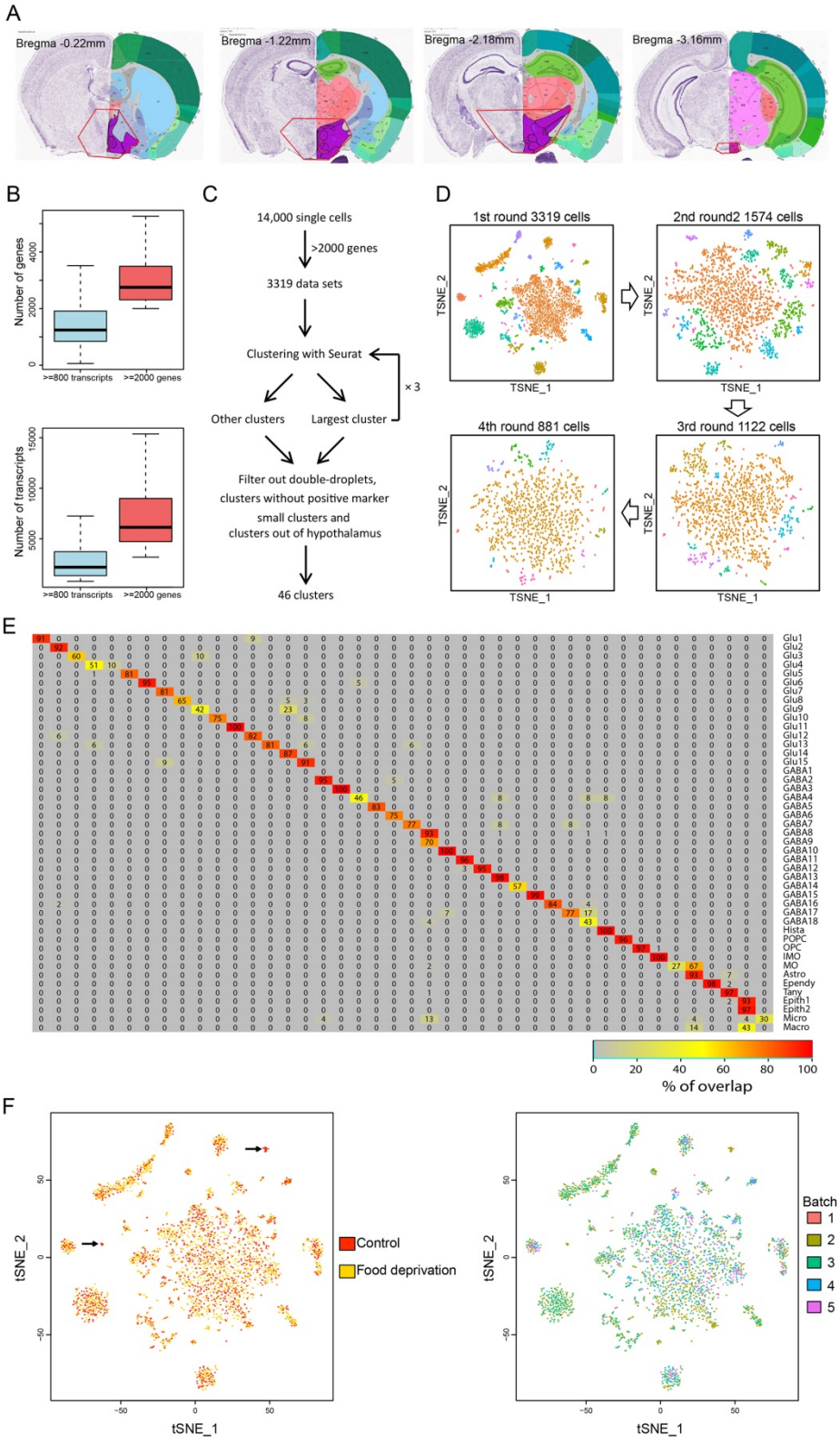

Figure S1 – Related to Figure 1. Workflow of single-cell RNA-seq of mouse hypothalamus

(**A**) Schematic diagram showing the hypothalamic regions used for sample preparation. Adult mouse brain was first cut into 1mm-thick coronal sections and then hypothalamic tissues (shown in red contours) were dissected from 4 successive slices along the rostral-caudal axis.

(**B**) Box plots showing the distribution of gene/transcript number detected in each single cell.

(**C**) Workflow of cell type classification. The entire dataset was analyzed to identify 3,319 cells with > 2000 different transcripts in each cell, which were then subjected to R package Seurat for classification. After each round of clustering, the cells in the largest cluster were subject to next round cluster analysis for a total of four rounds. All cell clusters were then pooled together and clusters with less than 10 cells, or representing double-droplets or without a marker identified or out of hypothalamus were filtered out. At the end, 45 cell clusters with distinct transcriptional features were identified.

(**D**) tSNE plots showing the results of different rounds of clustering. Distinct clusters are shown with different colors in each round.

(**E**) SC3 and Seurat generated similar clustering results. Heap map showing the pair-wise comparison of the clusters generated using Seurat and SC3. The x-axis represents clusters generated with SC3 and the y-axis represents clusters generated with Seurat. The number in each intersection represents the overlap between the two clustering results, which is color-coded.

(**F**) Distribution of cells from different treatments and different batches. tSNE plot showing the distributions of cells from different treatments (left panel) and different experimental batches (right panel). Different treatments or batches are represented with different colors. The two clusters indicated with arrows only contain cells from one control animal, which are excluded in our final clustering result because they were derived from brain regions out of hypothalamus.

Figure S2

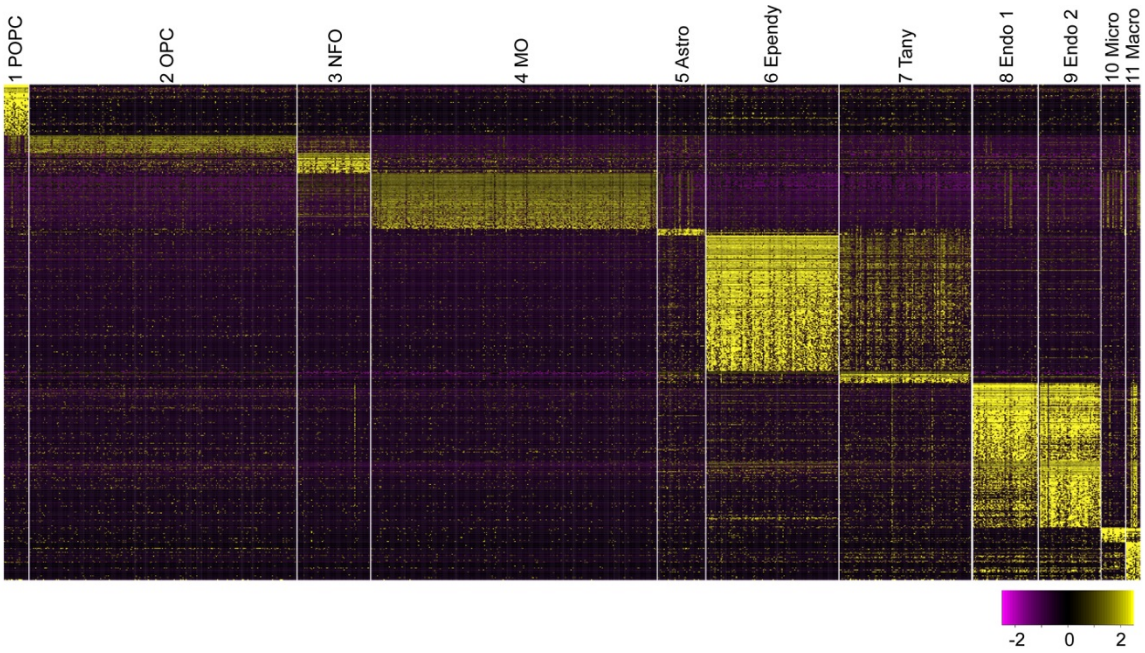
1 POPC
2 OPC
3 NFO
4 MO
5 Astro
6 Ependy
7 Tany
8 Endo 1
9 Endo 2
10 Micro
11 Macro
-2
0
2

Figure S2 – Related to Figure 2. Non-neuronal cell clusters feature distinct gene expression patterns

Heatmap showing the cell type-specific genes are differentially expressed across the 11 non-neuronal subtypes. Differentially expressed genes with power > 0.4, fold change > 2 among the 11 non-neuronal cell clusters were used to generate the heatmap. Columns represent individual cells and rows represent individual genes. The gene expression level is color-coded. POPC: proliferating oligodendrocyte progenitor cell; OPC: oligodendrocyte progenitor cell; NFO: newly formed oligodendrocytes; MO: myelinating oligodendrocyte; Astro: astrocyte; Ependy: ependymocyte; Tany: tanycyte; Endo: endothelial cell; Micro: microglia; Macro: macrophage.

Figure S3

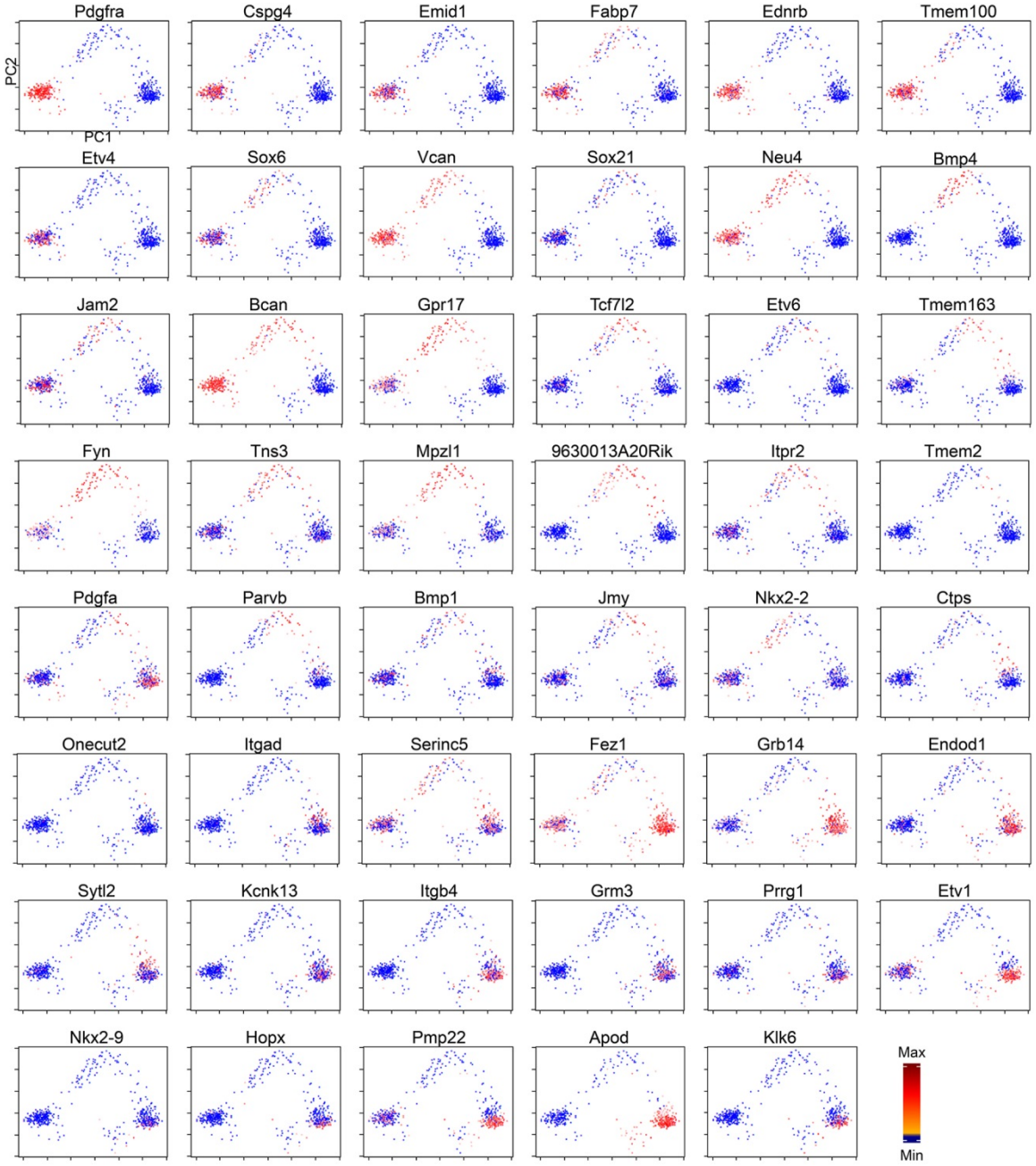
Pdgfra
Cspg4
Emid1
Fabp7
Ednrb
Tmem100
PC2
PC1
Etv4
Sox6
Vcan
Sox21
Neu4
Bmp4
Jam2
Bcan
Gpr17
Tcf7l2
Etv6
Tmem163
Fyn
Tns3
Mpzl1
9630013A20Rik
Itpr2
Tmem2
Pdgfa
Parvb
Bmp1
Jmy
Nkx2-2
Ctps
Onecut2
Itgad
Serinc5
Fez1
Grb14
Endod1
Sytl2
Kcnk13
Itgb4
Grm3
Prrg1
Etv1
Nkx2-9
Hopx
Pmp22
Apod
Klk6
Max
Min

Figure S3 - Related to Figure 3. Expression patterns of stage-specific genes during oligodendrocyte maturation

tSNE plots showing the expression patterns of stage-specific genes during oligodendrocyte maturation. The expression level is color-coded. For each gene, if the expression level in a cell is less than 5% of the max value of that gene in the whole cell population, the gene is considered as not expressed in that cell and is represented as a blue dot. The results are very similar to that obtained in a recent study (Marques et al., 2016).

Figure S4

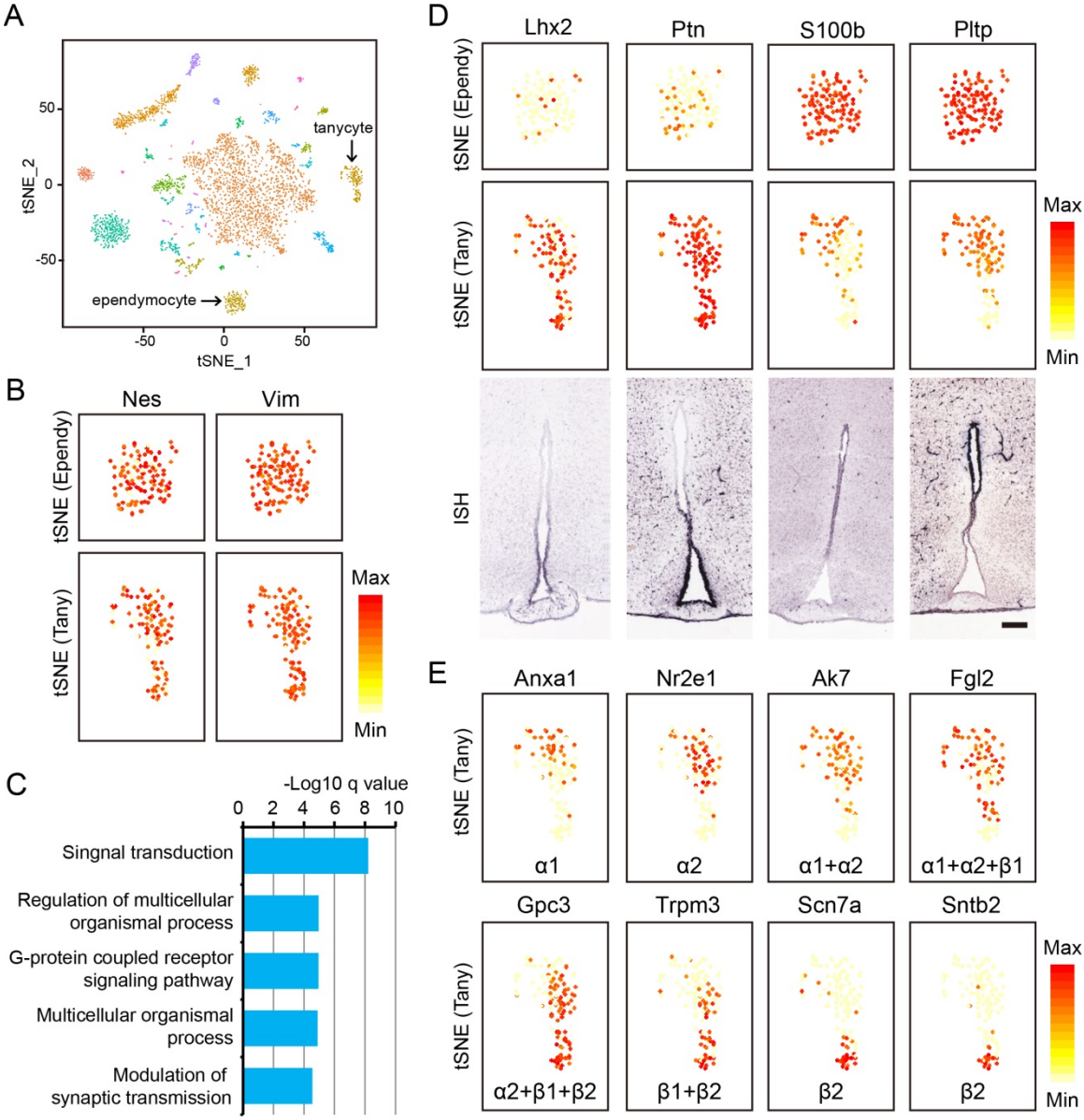
A
tanycyte
ependymocyte
tSNE_1
tSNE_2
B
Nes
Vim
tSNE (Ependy)
tSNE (Tany)
Max
Min
C
-Log10 q value
Singnal transduction
Regulation of multicellular organismal process
G-protein coupled receptor signaling pathway
Multicellular organismal process
Modulation of synaptic transmission
D
Lhx2
Ptn
S100b
Pltp
tSNE (Ependy)
tSNE (Tany)
ISH
Max
Min
E
Anxa1
Nr2e1
Ak7
Fgl2
α1
α2
α1+α2
α1+α2+β1
Gpc3
Trpm3
Scn7a
Sntb2
α2+β1+β2
β1+β2
β2
β2
tSNE (Tany)
Max
Min

Figure S4 - Related to Figure 4. Transcriptional features and gene expression heterogeneity of tanycytes

(**A**) tSNE plot presentation of the 3319 hypothalamic cells based on their transcriptomes indicates that tanycyte form a cell cluster that can be easily distinguished from the ependymocyte cluster.

(**B**) tSNE plots showing that *Nes* (nestin) and *Vim* (vimentin) are highly expressed in both ependymocyte (Ependy) and tanycyte (Tany). Gene expression level is color-coded.

(**C**) Enriched terms of the tanycyte cluster revealed by GO analysis. The hypergeometric-test was used.

(**D**) Expression patterns of selected tanycyte- and ependymocyte-specific genes. tSNE plots (upper and middle panels) and ISH data (lower panels, from Allen Brain Atlas) showing the differential expression patterns of genes in tanycytes (*Lhx2* and *Ptn*) and ependymocytes (*S100b* and *Pltp*). Gene expression level is color-coded. Scale bars, 200 μm.

(**E**) tSNE plots showing the expression of selected genes enriched in different subsets of tanycytes. The genes are ordered according to their expression level along the vertical axis of the tSNE map. For each gene, corresponding tanycyte subtype(s) are listed. Gene expression level is color-coded.

Figure S5

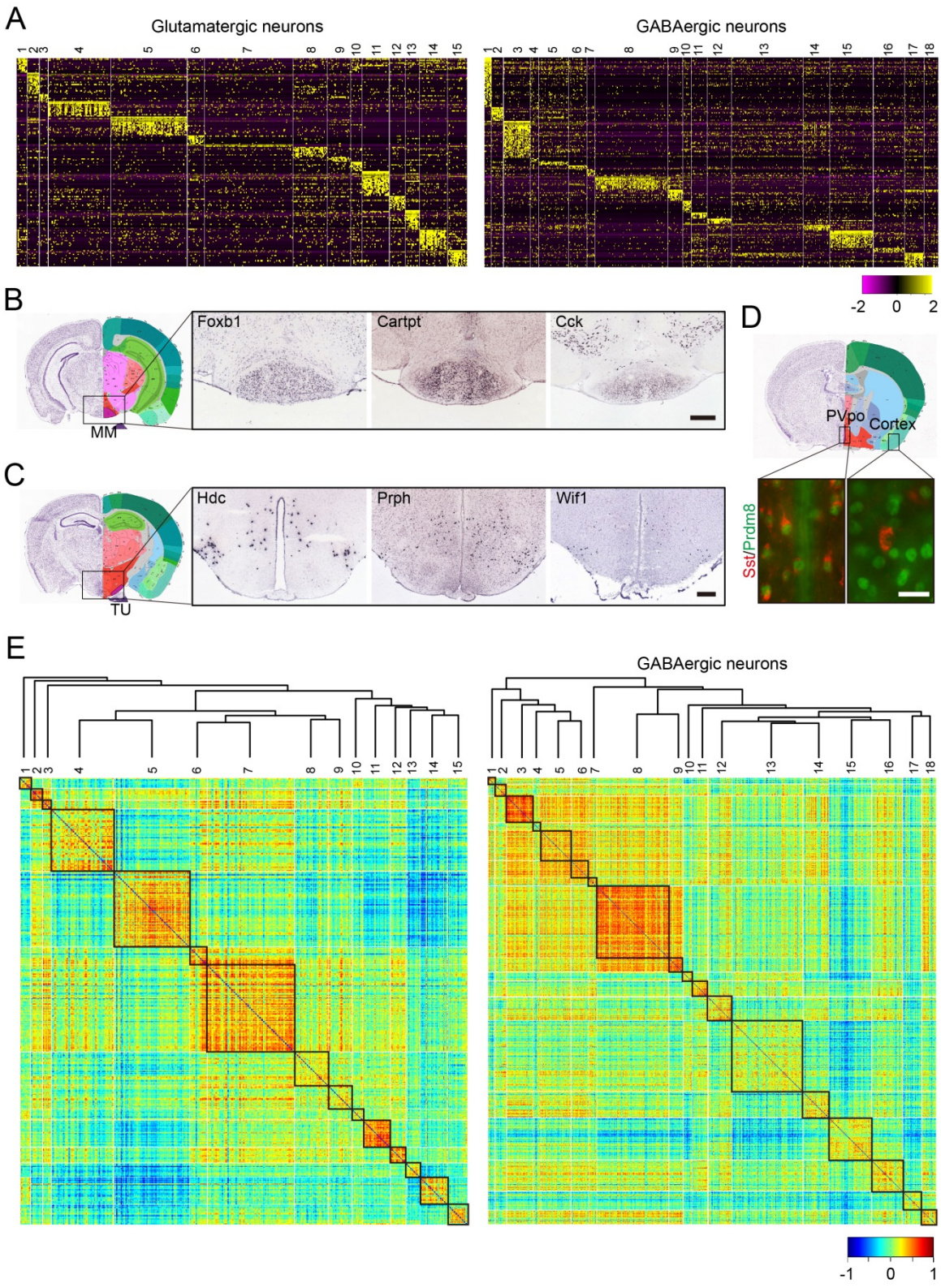
A
Glutamatergic neurons
GABAergic neurons
-2
0
2
B
Foxb1
Cartpt
Cck
MM
C
Hdc
Prph
Wif1
TU
D
PVpo
Cortex
Sst/Prdm8
E
GABAergic neurons
-1
0
1

Figure S5 - Related to Figure 5. Distinct expression patterns of hypothalamic neuronal cluster-specific genes

(**A**) Heatmaps showing the expression pattern of cell-type specific genes in the 15 glutamatergic and 18 GABAergic neurons clusters. Differentially expressed genes with power > 0.4, fold change > 2 among the glutamatergic or GABAergic clusters were used to generate the heatmap. Columns correspond to individual cells and the numbers above the heatmaps indicate cluster identity. Rows represent individual genes and expression level is color-coded.

(**B**) ISH data (from Allen Brain Atlas) showing the expression of *Foxb1*, *Cartpt* and *Cck* in MM. The contour region in the left panel is enlarged and shown in the right three panels. MM, mammillary body. Scale bars, 300 μm.

(**C**) ISH data (from Allen Brain Atlas) showing the expression of *Hdc*, *Prph* and *Wif1* in TU. The contour region in the left panel is enlarged and shown in the right three panels. TU, tuberal nucleus. Scale bars, 300 μm.

(**D**) Immunostaining showing co-localization of Sst and Prdm8 in PVpo but not in cortex. The lower panels represent corresponding boxed regions in the upper panel. Scale bars, 40 μm.

(**E**) Clustering relationship of the 15 glutamatergic and 18 GABAergic neuron subtypes. The dendrograms indicate the relatedness among neuron subtypes based on gene expression. Differentially expressed genes with SD > 2 are used to generate the hierarchical clustering trees and cell-cell similarity heatmaps. The numbers on the top of the heatmaps indicate cluster identity.

Figure S6

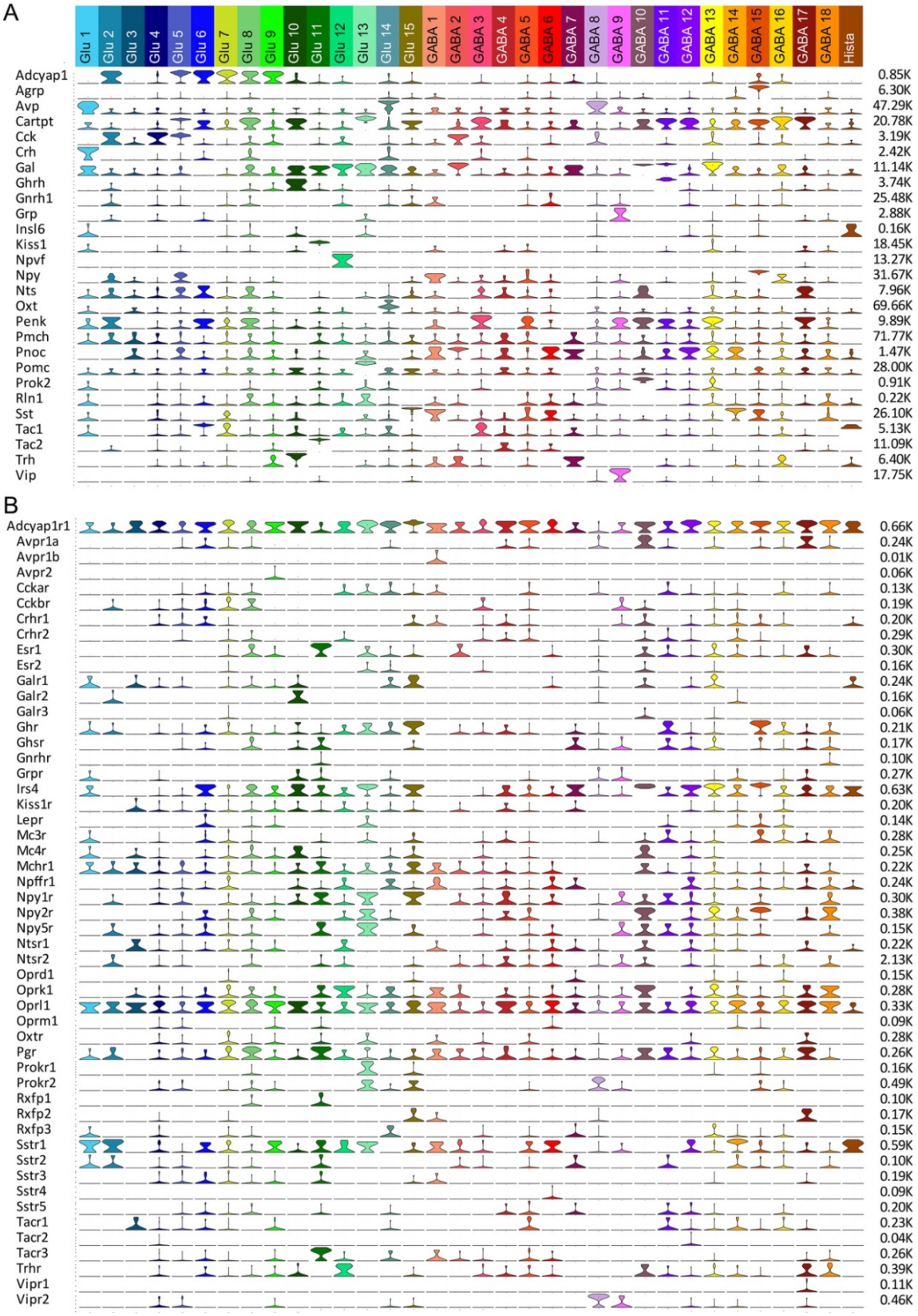
A
Glu 1
Glu 2
Glu 3
Glu 4
Glu 5
Glu 6
Glu 7
Glu 8
Glu 9
Glu 10
Glu 11
Glu 12
Glu 13
Glu 14
Glu 15
GABA 1
GABA 2
GABA 3
GABA 4
GABA 5
GABA 6
GABA 7
GABA 8
GABA 9
GABA 10
GABA 11
GABA 12
GABA 13
GABA 14
GABA 15
GABA 16
GABA 17
GABA 18
Hista
Adcyap1 0.85K
Agrp 6.30K
Avp 47.29K
Cartpt 20.78K
Cck 3.19K
Crh 2.42K
Gal 11.14K
Ghrh 3.74K
Gnrh1 25.48K
Grp 2.88K
Insl6 0.16K
Kiss1 18.45K
Npvf 13.27K
Npy 31.67K
Nts 7.96K
Oxt 69.66K
Penk 9.89K
Pmch 71.77K
Pnoc 1.47K
Pomc 28.00K
Prok2 0.91K
Rln1 0.22K
Sst 26.10K
Tac1 5.13K
Tac2 11.09K
Trh 6.40K
Vip 17.75K
B
Adcyap1r1 0.66K
Avpr1a 0.24K
Avpr1b 0.01K
Avpr2 0.06K
Cckar 0.13K
Cckbr 0.19K
Crhr1 0.20K
Crhr2 0.29K
Esr1 0.30K
Esr2 0.16K
Galr1 0.24K
Galr2 0.16K
Galr3 0.06K
Ghr 0.21K
Ghsr 0.17K
Gnrhr 0.10K
Grpr 0.27K
Irs4 0.63K
Kiss1r 0.20K
Lepr 0.14K
Mc3r 0.28K
Mc4r 0.25K
Mchr1 0.22K
Npffr1 0.24K
Npy1r 0.30K
Npy2r 0.38K
Npy5r 0.15K
Ntsr1 0.22K
Ntsr2 2.13K
Oprd1 0.15K
Oprk1 0.28K
Oprl1 0.33K
Oprm1 0.09K
Oxtr 0.28K
Pgr 0.26K
Prokr1 0.16K
Prokr2 0.49K
Rxfp1 0.10K
Rxfp2 0.17K
Rxfp3 0.15K
Sstr1 0.59K
Sstr2 0.10K
Sstr3 0.19K
Sstr4 0.09K
Sstr5 0.20K
Tacr1 0.23K
Tacr2 0.04K
Tacr3 0.26K
Trhr 0.39K
Vipr1 0.11K
Vipr2 0.46K

Figure S6 - Related to Figure 6. Expression of neuropeptides and receptors across neuronal subtypes

(**A**) Violin plot showing the expression profile of different neuropeptides (rows) across the hypothalamic neuronal subtypes (columns). Gene expression level is shown on a linear scale and adjusted for each gene with the maximum TPM value indicated on right.

(**B**) Violin plot showing the expression profile of different neuropeptide receptors (rows) among the hypothalamic neuronal subtypes (columns).

Figure S7

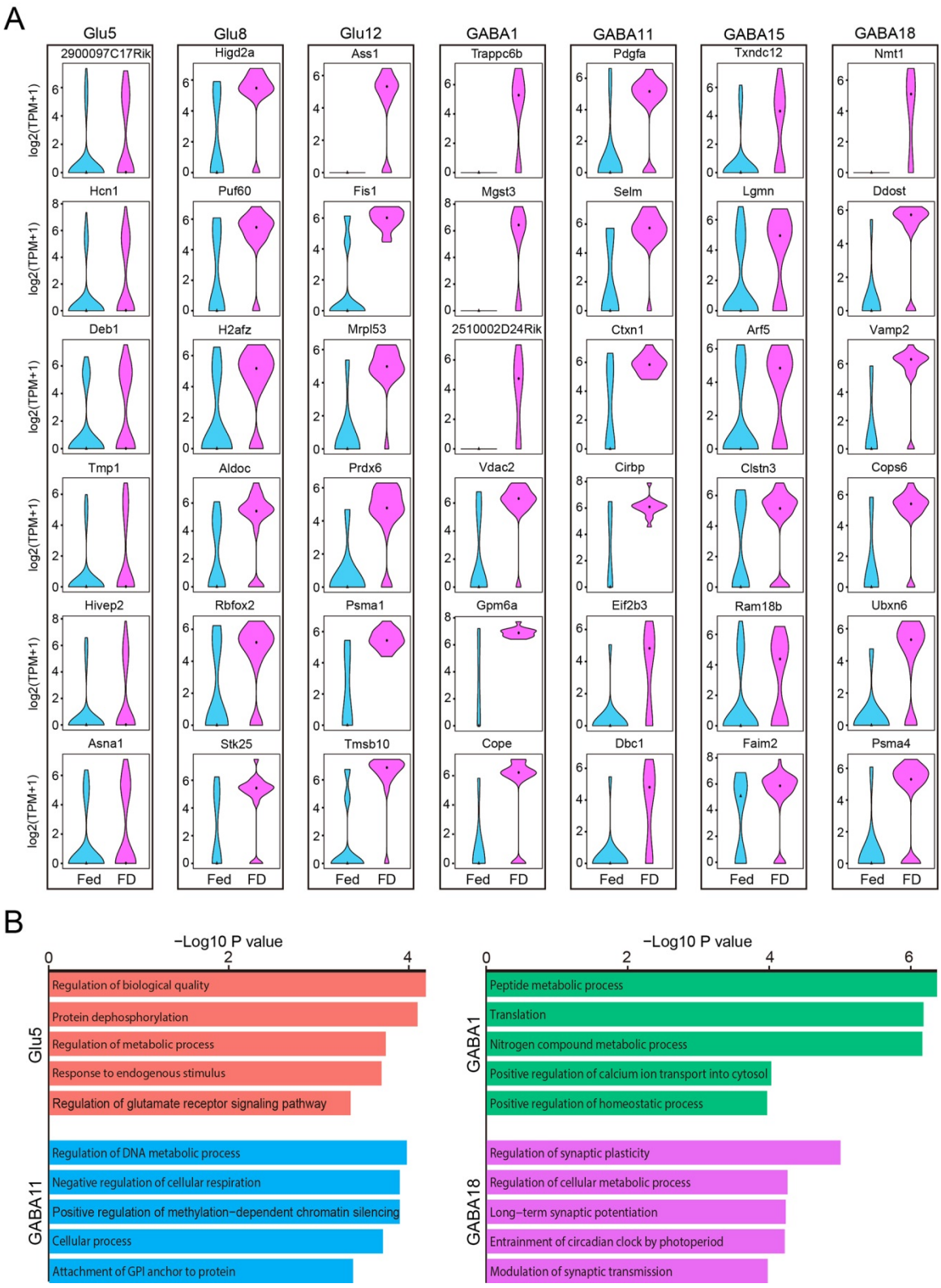
A
Glu5
Glu8
Glu12
GABA1
GABA11
GABA15
GABA18
2900097C17Rik
Higd2a
Ass1
Trappc6b
Pdgfa
Txndc12
Nmt1
Hcn1
Puf60
Fis1
Mgst3
Selm
Lgmn
Ddost
Deb1
H2afz
Mrpl53
2510002D24Rik
Ctxn1
Arf5
Vamp2
Tmp1
Aldoc
Prdx6
Vdac2
Cirbp
Clstn3
Cops6
Hivep2
Rbfox2
Psma1
Gpm6a
Eif2b3
Ram18b
Ubxn6
Asna1
Stk25
Tmsb10
Cope
Dbc1
Faim2
Psma4
log2(TPM+1)
Fed
FD
B
−Log10 P value
Regulation of biological quality
Protein dephosphorylation
Regulation of metabolic process
Response to endogenous stimulus
Regulation of glutamate receptor signaling pathway
Glu5
Regulation of DNA metabolic process
Negative regulation of cellular respiration
Positive regulation of methylation−dependent chromatin silencing
Cellular process
Attachment of GPI anchor to protein
GABA11
Peptide metabolic process
Translation
Nitrogen compound metabolic process
Positive regulation of calcium ion transport into cytosol
Positive regulation of homeostatic process
GABA1
Regulation of synaptic plasticity
Regulation of cellular metabolic process
Long−term synaptic potentiation
Entrainment of circadian clock by photoperiod
Modulation of synaptic transmission
GABA18

Figure S7 - Related to Figure 7. Food deprivation-induced transcription changes in different hypothalamic neuron clusters

(**A**) Violin plots showing representative genes in different neuronal subtypes that are induced by food deprivation. Each column represents one neuron cluster. Gene expression level is shown on a log scale. For the fold change and p-value of each gene, see Table S7. Fed, normal feeding; FD, food deprivation.

(**B**) GO enrichment analysis of representative neuronal clusters that exhibit high numbers of gene transcriptional changes. The hypergeometric-test was used. Also see Table S8.

Supplemental Tables

Table S1 - Related to Figure 1 - Summary of the clustering results

Table S2 - Related to Figure 3 - Six groups of genes dynamically expressed during oligodendrocyte differentiation

Table S3 - Related to Figure 3 - GO results of the six groups of genes with dynamic expression during oligodendrocyte differentiation

Table S4 - Related to Figure 4 - Differentially expressed genes in tanycyte and ependymoctye

Table S5 - Related to Figure 5 - Maker genes of neuronal clusters

Table S6 - Related to Figure 7 - Summary of scRNA-seq comparing transcriptome of hypothalamic neuron clusters from normal and food-deprived mice

Table S7 - Related to Figure 7 - GO analyses of genes in different hypothalamic neuron subtypes affected by food deprivation

Supplemental Experimental Procedures

Animals

All animal experiments followed the guidelines of the Institutional Animal Care and Use Committee at Harvard Medical School. Young adult female (8 - 10 weeks) B6D2F1 mice (C57B6 female × DBA2 male) were used. One day before the experiments, each animal was separated into individual fresh cages. For 24 h food deprivation treatment, only water was provided. In total 4 control animals and 3 food-deprived mice were used for single-cell RNA sequencing. All single-cell RNA-seq experiments were performed in five batches within 3 months. Each animal was processed separately (cell dissociation, library preparation) and regarded as a biological replicate.

Tissue dissection and dissociation

For hypothalamus dissection, the mice were anesthetized and the entire brain was removed and transferred into ice-cold Hibernate A/B27 medium (60 ml Hibernate A medium with 1 ml B27 and 0.15 ml Glutamax). The coronal sections from Bregma -0.22 to – 3.16 mm were then cut with brain matrix and further sliced into 1 mm slices. Hypothalamic tissue was then dissected from each slice under dissection microscope and subjected to tissue dissociation (Figure S1A). The hypothalamic tissues were dissociated into single-cell suspension using a papain-based dissociation protocol (Brewer and Torricelli, 2007) with some modifications. Briefly, the hypothalamic tissues from each mouse were cut into small pieces and incubated in Hibernate A-Ca medium with 2 mg/ml papain at 30^0C for 40 min with constant agitation. After washing with 5 ml Hibernate A/B27 medium, the tissues were triturated with fire polished glass Pasteur pipettes into a single-cell suspension within 6 ml Hibernate A/B27 medium. To remove debris, the single-cell suspension was loaded on a 4-layer OptiPrep gradient and centrifuged at 800 g for 15 min at 4^0C. Fractions 2 – 4 were then collected and washed with 5 ml Hibernate A/B27 medium and 5 ml DPBS with 0.01% BSA. In some experiments (batch 4 and 5), only fraction 3 is collected to enrich neurons. The cells were spun down at 200 g for 3

min and re-suspended in 0.4 ml DPBS with 0.01% BSA. A 10 µl cell suspension was stained with Trypan Blue and the live cells were counted. During the entire procedure, the tissues or cells were kept in ice-cold solutions except for the papain digestion.

Single cell capture, library preparation, and sequencing

Single cells and barcoded beads were captured into nanoliter-sized droplets as previously described (Macosko et al., 2015). The hypothalamic cell suspension was diluted to 100 cells/µl with DPBS containing 0.01% BSA and 0.6 – 1 ml cell suspension was loaded in each experiment. After cell capture, reverse transcription, cDNA amplification and sequencing library preparation were perform as described (Macosko et al., 2015). Sequencing was performed using Illumina Hiseq 2500 sequencer. Raw sequencing reads were analyzed using the Drop-seq software (Macosko et al., 2015) (http://mccarrolllab.com/dropseq/). Transcript count for each gene was converted to transcripts per million (TPM) for downstream analysis.

Cell clustering

The R package Seurat was used for cell clustering analysis (Macosko et al., 2015). To determine the optimal cut-off that balances data quality and cell numbers, we tried different cut-offs (detect expression of 800, 2000, and 2500 genes in each single cell) and found that 2000-gene cut-off gave the best results, thus we used the 3319 cells with 2000 or more gene expression detectable for clustering analysis. The highly variable genes were identified from these cells using Seurat with the default setting followed by principle component analysis (PCA). Then the statistically significant PCs ($p<0.05$) were used for 2-dimension tSNE. Based on the tSNE map, density-based clustering (DBSCAN) was used to cluster cells based on their proximity (G.use=3), resulting in 40 clusters with a large neuronal cluster containing 1574 cells. We reasoned that the PCs used for the first round clustering might be mainly comprised of non-neuronal cells and some specific neuronal subtypes. The majority of neurons, despite having subtype-specific genes, may have more closely related transcriptomes that form the large neuronal cluster. To separate the large cluster, we extracted cells within the cluster for further clustering using the

same strategy described above. The same analysis was repeated for an additional two times. After four rounds of clustering, a total of 73 cell clusters were identified.

Filter the initial clustering results

We applied the follow criteria to filter out initial clustering results: 1) marker genes were identified for all of the clusters with the function markers.all in R package Seurat; If a positive marker (marker gene enriched in a certain cluster compared with other clusters) cannot be found for a cluster, the cluster was excluded; 2) If a cluster co-expresses both non-neuronal and neuron markers, or non-neuronal markers of different subtypes, or glutamatergic and GABAergic markers (*Slc17a6* and *Slc32a1*), then the cluster is excluded as the cluster likely represent double-droplets; 3) Clusters with less than 10 cells were excluded, which can further remove very small neuron clusters which may represent neuron-neuron double-droplets; 4) By manually checking the expression pattern of makers for each cluster in mouse brain (Allen Brain Atlas), clusters from brain regions out of hypothalamus (e.g. thalamus) were excluded. This criterion was used to exclude non-hypothalamic cell clusters from non-hypothalamic tissue. After filtering, a total of 45 cell clusters were identified.

Seurat and SC3 clustering results comparisom

We applied SC3 to classify the 3319-cell dataset, which calculates consensus for each value of k and averages the clustering results of k-means using a consensus approach (Kiselev et al., 2016). Briefly, UMI counts of 3319-cell dataset were considered as count data to construct a new object with R package scater. QC metrics were computed for the created object and data filtering was performed with default parameters. To get clustering results with SC3, we started with function sc3_prepare. This method prepares an object of SCESet class for SC3 clustering. Function sc3_calc_distscalculates in SC3 package calculates the distances, including Euclidean, Pearson and Spearman distances. Function sc3_calc_transfs in SC3 package calculates transformation of the distance matrices corresponding to PCA and graph Laplacian transformations. K-means was then performed on the transformed distance matrices with function sc3_kmeans in SC3 package. Function Sc3_calc_consens in SC3 package calculates consensus matrices

based on the clustering solutions. To estimate the best K, function sc3_estimate_k in SC3 package which utilizes the Tracy-Widom theory on random matrices was used. The preliminary analysis with optimal K=27 shows that the majority of the cluster are not stable based on Silhouette plot or contain subpopulation structure based on manually checking the consensus matrix. Then a wide range of K from 27 to 150 was used to get different clustering solutions. For a given cluster from Seurat the maximum recovery rate was estimated across the different K values. Then a non-overlapping maximum recovered consensus cluster solution was generated as final clustering results. By calculating the overlap of cells across different clusters generated by Seurat and SC3, we found these two methods generate very similar clustering results (**Figure S1E**).

Predict cell identities for each of the 14,437 sequenced cells with Svm

Function markers.all in R package Seurat was used to identify cluster marker genes using the 3319 cell-derived dataset (ROC test). All marker genes with power less than 0.4 were discarded. The 3319 cells were fed to the function svm as the training dataset to build a classifier based on 3587 marker genes. Then function prediction was used to assign each of the 14437 cells (>= 800 transcripts in each cell) to one cluster based on transcriptional similarity. A total of 14437 cells were then subject to identified marker genes using function markers.all in R package Seurat. In total 1430 genes with at least 5-fold change were identified.

Analysis of the oligodendrocyte and tanycyte clusters

To analyze the timing of differentiation in oligodendrocytes, we extracted cells belonging to oligodendrocyte precursor cell, newly formed oligodendrocyte and myelinating oligodendrocyte clusters from the 3319-cell dataset (2000-gene cut-off). The three subpopulations were pooled for analysis. The 768 most variable genes among all the single cells were identified by Seurat (ROC test, power>0.4) (Macosko et al., 2015). A pseudo developmental timeline of single cells was then calculated with the package Monocle (Trapnell et al., 2014), using the most variable genes as time ordering genes. Based on the established differentiation direction of oligodendrocyte (from OPC to NFO to MO), the direction of pseudotime axis was determined. In Figure 3C, the six groups of

genes displaying six temporal patterns during the three developmental stages were identified by Seurat (ROC test, power>0.4). GO Term analysis of these six groups of genes was performed using Gorilla (Eden et al., 2009). All analyses for tanycyte and ependymal cells were based on the 3319-cell dataset. Identification of the differentially expressed genes between tanycyte and ependymocyte were carried out using Seurat (ROC test, power>0.4) (Macosko et al., 2015). GO term analysis were performed using Gorilla (Eden et al., 2009). Identification of the differentially expressed genes within tanycyte population and principle component analysis (PCA) were performed with Seurat (Macosko et al., 2015).

tSNE plot, dendrogram and heatmap for glutamatergic and GABAergic clusters

Neurons belonging to clusters Glu1-15 and GABA1-18 were extracted from the 3319-cell dataset and new Seurat objects were built using function setup for glutamatergic neurons and GABAergic neurons, respectively. The marker genes were identified by using the function find_all_markers of Seurat package (ROC test, requiring power > 0.4, fold change > 2), which was used for constructing a gene expression matrix for tSNE plot and heatmap. Rtsne with parameters of 'pca = TRUE, max_iter = 2000, perplexity = 30' was used to build a 2D map for visualization. Each dot represented a single cell and each cluster was colored with scheme consistent with other figures. Heatmaps in Figure S5A was generated by function doHeatMap. To generate the dendrograms presented in Figure S5E, variable genes with SD > 2 within glutamatergic or GBABergic neurons were selected, and the mean values of those genes in each cluster were then calculated. Hierarchical clustering was performed with R function dist and hclust (method="ward.D2") based on mean values of variable genes. To generate the cell-cell similarity heatmap in Figure S5E, the gene set which were used to generate Figures 5A and 5B were used. The expression TPM value of each gene was transformed to log2 value and scaled. Spearman correlation of each pair of cells was calculated by R function RCORR. Then R function heatmap.2 was used to generate the heatmap.

Identification of food deprivation affected genes

Base on the clustering results of 14,437 cells, within each neuronal cluster, the number of cells from "Fed" (ad libitum fed) and "FD" (food-deprived) mice are calculated. Clusters have at least 4 cells from both "Fed" and "FD" group are subjected to further analysis. lrTest function (likelihood ratio test) in R package MAST was used to calculate P value with "hurdle" model for comparing gene expression level. Genes with fold change > 1.5 and P value < 0.01 are defined as differentially expressed genes. GO analysis are performed with Gorilla (Eden et al., 2009) with default parameters. All gene symbols in mouse genome are used as background gene set. Redundant GO terms are manually removed.

Immunostaining

Anesthetized mice (8 -10 week) were perfused with PBS followed by 4% paraformaldehyde (PFA) in PBS. The whole brain was removed and fixed in 4% PFA overnight followed by 30% sucrose in PBS for 24h at 4^0C. Coronal sections were cut at 30 μm with cryostat and stored in PBS before use. A free-floating procedure was used for immunostaining. Briefly, brain slices containing the regions of interest were blocked in 5% BSA and 0.3% Triton-X 100 in PBS for 1 h at room temperature before being incubated in primary antibodies in blocking buffer overnight at 4^0C. After washing 3 times for 15 min in PBS, sections were incubated in blocking buffer containing secondary antibodies and DAPI at room temperature for 2 h, followed by washing 3 times with PBS. Brain slices were then attached to slides and coverslips were applied. The Sst antibody (rabbit, 1:100) was from Invetrogen, the Pax6 antibody (rabbit, 1:300) was from Covance, the Prdm8 antibody (guinea pig, 1:1000) was a gift from Dr. Sarah E. Ross (Ross et al., 2012), the Agrp antibody (goat, 1:100) was from Santa Cruz, the Cirbp (goat, 1:100), Crabp1 (mouse, 1:200) and Trim28 (mouse, 1:100) antibodies were from Abcam.